Report No. 03-66-21

FINAL PROJECT REPORT

on

ADVANCEMENT OF THE STATE-OF-THE-ART IN THE PRODUCTION OF DRIFT FIELD SOLAR CELLS

23 June 1965 to 23 January 1966
Contract No. NAS5-9609

Prepared by

Texas Instruments Incorporated
Semiconductor-Components Division
P. O. Box 5012
Dallas, Texas 75222

for

National Aeronautics and Space Administration
Goddard Space Flight Center
Glenn Dale Road
Greenbelt, Maryland 20771

FINAL PROJECT REPORT

on

ADVANCEMENT OF THE STATE-OF-THE-ART
IN THE PRODUCTION OF DRIFT FIELD SOLAR CELLS

23 June 1965 to 23 January 1966
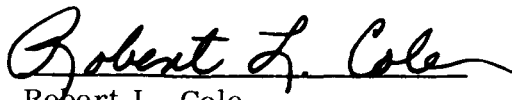Contract No. NAS5-9609

Prepared by

Texas Instruments Incorporated
Semiconductor-Components Division
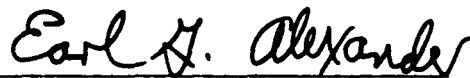P. O. Box 5012
Dallas, Texas 75222

for

National Aeronautics and Space Administration
Goddard Space Flight Center
Glenn Dale Road
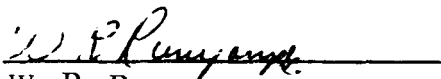Greenbelt Road, Maryland 20771

Robert L. Cole
SPB Program Engineer

Earl G. Alexander
MTB of SRDL, Project Engineer

Larry G. Sloan
Manager, Manufacturing and
Engineering, SPB

W. R. Runyan
Manager, Materials Technology Branch

J. S. Kilby, Deputy Director
Semiconductor Research and Development
Laboratory

FOREWORD

This is the final report of work performed under Contract No. NAS 5-9609. The work was performed and this report was prepared jointly by the Special Products branch (SPB) within the General Products department and by the Materials Technology branch (MTB) of the Semiconductor Research and Development Laboratory. These organizational units are in the Semiconductor-Components (S-C) division of Texas Instruments Incorporated.

Mr. Robert L. Cole and Dr. Earl G. Alexander were project engineers for work performed within the SPB and MTB, respectively. Dr. W. R. Runyan of MTB served as consultant. Surface preparation and sawing operations were carried out under the direction of Mr. Richard L. Yeakley and Mr. Jimmie B. Sherer of MTB. Fabrication and testing operations were directed by Mr. Raymond A. Vineyard of SPB. Impurity profile studies were performed by Mr. Stacy B. Watelski of MTB, assisted by Mr. Ronald C. Wackwitz of the Management Systems department of S-C who provided computer programming and routines. Mr. Richard H. Kinsey was contract administrator.

The work was performed under the administration of Mr. M. Schach and Dr. P. H. Fang of the Goddard Space Flight Center, Greenbelt, Maryland. Irradiation data were supplied through their courtesy.

SUMMARY

Various works have indicated that a solar cell fabricated to include a drift-field structure should be more resistant to electron radiation than an ordinary n/p cell. The objective of this contract has been to improve existing methods for producing such cells, to evaluate the earlier theoretical work, and to improve an existing technique for profiling the concentration gradient present in the drift-field structure.

Six lots of experimental drift-field solar cells were fabricated and supplied to NASA-Goddard for radiation experiments. In the preparation of these cells, basic drift-field parameters, such as location, width, and magnitude of the drift-field were varied and manufacturing conditions were held constant. Standard epitaxial material was used for starting material, and the manufacturing process could easily be adapted to production. Sample cells were characterized before and after irradiation, by current, voltage, and spectral response measurements. The improved impurity concentration profile technique represents an important advance in drift-field evaluation.

Relative behavior of the various cell groups before irradiation quite closely follows previously developed theory for drift field cells. The cells after irradiation (to 10^{16} one MeV electrons/cm^2), however, behave as if they had no field. The present data appear to be quite clear, the theory predicting enhancement appears to be in order, and the profiling measuring technique shows the drift-field structure to be located correctly. The constant that relates lifetime to total flux is impurity-concentration dependent. Since the magnitude of the change seems capable of producing considerable additional lifetime degradation in the concentration gradient region, the effect of the field, introduced by the gradient, may be completely negated.

Over the range of total flux considered in this study, there appears to be little advantage in using drift-field cells.

TABLE OF CONTENTS

LIST OF ILLUSTRATIONS (Continued)

LIST OF TABLES

SECTION I

INTRODUCTION

Various theoretical and experimental works have indicated that a solar cell fabricated to include a drift-field structure should be more resistant to hard particle radiation than an ordinary n/p cell. Texas Instruments and several other organizations have been engaged in various drift-field studies for several years. Progress by Texas Instruments in the performance of Contract No. NAS5-3559 indicated the feasibility of using epitaxial structures for constructing drift-field solar cells. Detailed calculations completed under that contract[1] have shown that there is an optimum field width for a given residual lifetime (radiation dosage), and that the upper and lower concentration limits in the impurity gradient which produces the field should differ by at least three orders of magnitude. These calculations were made on the basis of optimizing the short-circuit electron current from the p-region of the cell.

The purpose of the present contract was to advance the state-of-the-art in producing drift-field cells of improved resistance to the effects of radiation experienced in a space environment. Such cells would have significant value on high radiation environment satellite and probe missions.

The program was carried out by fabricating experimental lots of solar cells in which basic drift-field parameters were varied and manufacturing conditions were constant. Parameters considered to be most important were location, width, and

---

[1] Texas Instruments Incorporated, Technical Summary Report 03-65-77, "Development of Epitaxial Structures for Radiation Resistant Silicon Solar Cells," dated July 1965, Contract No. NAS5-3559.

magnitude of the drift-field. Sample solar cells were submitted to NASA (Goddard Space Flight Center) for radiation testing and evaluation to determine optimum design parameters. Also included in the scope of the contract was improvement of the concentration gradient profile technique developed in the previous contract.

The work on this contract was performed jointly by the Special Products branch (SPB) within the General Products department of the Semiconductor-Components (S-C) division and the Semiconductor Research and Development Laboratory (SRDL) of the S-C division. The SRDL group prepared the drift-field structure material and the SPB group performed all fabrication steps from diffusion to final electrical test. Impurity profile studies and analysis of the radiation data were also made by SRDL.

Because this work is a continuation of a program begun under a previous contract, there is much background information that is not repeated here but which may be found in the final report of Contract No. NAS5-3559[1/].

SECTION II

EPITAXIAL RESULTS AND INITIAL CELL CHARACTERISTICS

A.   GENERAL

Epitaxial structures were prepared and diffused to provide six lots of material from which drift-field solar cells were fabricated. A schematic structure of the drift-field silicon slice before assembly into a solar cell is shown in Figure 1. Drift fields were formed by diffusing substrate impurities (initial concentration N_2) into the epitaxial layer (initial concentration N_1) of thickness t such that the diffusion front reaches to the surface. This method has been described in considerable detail in Section III, Part C of Reference 1.

The epitaxial slices were obtained as a standard commercial item from the Chemical Materials department of TI's Materials and Controls division. Ordering specifications for the optimum cell (Lot 3) are given in Appendix I.

The six lots provided a range of drift-field widths and impurity gradients for evaluation. Table I lists values of the basic parameters which were being varied for the six lots. The time-temperature diffusion conditions used to diffuse the substrate impurities the required amount are given in the last two columns. Due to the thinness of the epitaxial layers of Lot 1 (5 μm) and the fast rate of diffusion of aluminum (in Lot 6), Lots 1 and 6 were each divided into two sub-lots, and each sub-lot was diffused for a different period of time.

Cells were fabricated from the various lots, and ten sample cells from each lot were shipped to NASA-Goddard for irradiation testing. Sub-lots 1A, 1B, 6A, and 6B contained five cells each.

Table I. Epitaxial and Drift-diffusion Conditions for Solar Cell Material

NASA Lot Number	Silicon Substrate Dopant	Silicon Substrate* Resistivity (Ω-cm)	N_2 (cm^{-3})	Nominal Epitaxial Layer** Resistivity (Ω-cm)	N_1 (cm^{-3})	Nominal Epitaxial Layer Thickness (μm)	Diffusion Hours	Diffusion Temp. °C
1 A	Boron	0.06	1.0×10^{18}	3	4.5×10^{15}	5	1.25	1250
1 B	Boron	0.06	1.0×10^{18}	3	4.5×10^{15}	5	1.66	1250
2	Boron	0.06	1.0×10^{18}	9	1.5×10^{15}	12	7.00	1250
3	Boron	0.06	1.0×10^{18}	8	1.7×10^{15}	25	28.25	1250
4	Boron	0.008	1.4×10^{19}	9	1.5×10^{15}	12	4.10	1250
5	Boron	0.20	1.6×10^{17}	9	1.5×10^{15}	12	22.40	1220
6 A	Aluminum	0.06	1.0×10^{18}	10	1.4×10^{15}	12	0.42	1250
6 B	Aluminum	0.06	1.0×10^{18}	10	1.4×10^{15}	12	0.25	1250

* Substrates were Czochralski pulled.

** Epitaxial films were boron-doped.
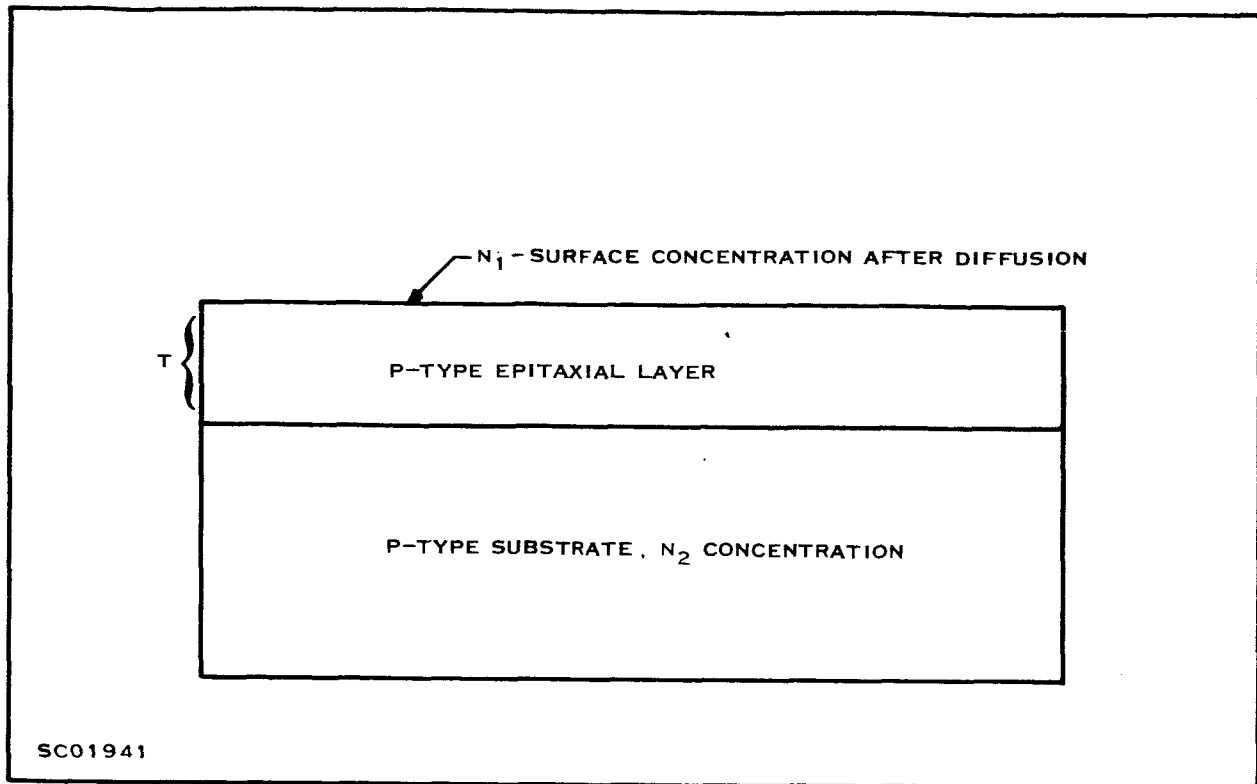
Figure 1. Drift-field Silicon-slice Structure

B.   INITIAL CURRENT-VOLTAGE CHARACTERISTICS

Current-voltage curves for the best sample cell from each group (as shipped) are given in Figures 2 through 9. The average values of the initial electrical characteristics of sample cells delivered to NASA are displayed in Table II. (Average values are given because of the small amount of scatter and to facilitate data presentation.) Values of open circuit voltage (V_{oc}) for cells in sub-lot 1A are virtually identical to those in sub-lot 1B. V_{oc} values for sub-lots 6A and 6B also are identical. Thus, for these lots, the position of the drift-field, relative to the front surface, does not appear to influence the value of V_{oc}. Because of the closeness of their characteristics, sub-lots 1A and 1B and sub-lots 6A and 6B are consolidated for the remainder of this report into two lots.

Table II. Initial Electrical Characteristics of
Sample Cells Delivered to NASA

NASA Lot Number	Average Values		
	I_{sc} (mA)	V_{oc} (mV)	Max. Percent Efficiency*
1A	37.4	568	7.9
1B	39.1	568	8.3
2	45.0	590	10.7
3	48.1	583	11.1
4	35.1	575	7.7
5	50.8	595	12.2
6A	37.7	543	8.0
6B	39.0	545	8.4

* Based on 1.8 cm^2 active area.

Distributions of short-circuit current (I_{sc}) values for the various lots are shown in Figure 10. All cells in the process run, not just the sample cells, are included in these data. Significant differences in values of I_{sc} are apparent. For cells made on 0.06 Ω-cm, boron-doped substrates (Lots 1, 2, 3), values of I_{sc} increase with increasing width of the drift field. Similar results were reported in Reference 1 for cells made on 0.008 Ω-cm substrates. This behavior is as predicted by theory, and arises because many of the carriers are generated in the low mobility region of the cell, and because the narrow aiding field does not extend to the generation point. Thus, the carriers recombine before reaching the junction. The reason for the low mobility region is explained in detail in Reference 1; but briefly, it is due to the additional doping required to produce the aiding drift field.

At a constant drift-field width of about 12 μm, values of I_{sc} increase with increasing resistivity of the substrate (Lots 4, 2, 5). Cells made on the aluminum-doped

substrates (Lot 6) exhibit I_{sc} values that are about 6 mA lower than those in the comparable boron-doped group (Lot 2). A definite reason for this difference is not known, but the aluminum-doped silicon crystal may have had a lower lifetime. Highest values of I_{sc} occur for cells in Lots 3 and 5, for which the drift fields are closest in design to the "optimum" structure reported in Reference 1 for an irradiated cell.

C. INITIAL QUANTUM YIELD MEASUREMENTS

Quantum-yield measurements made by NASA permit a plot of wavelength response before irradiation. From two to four sample cells in each group were measured; Figure 11 shows the average value for each lot. A comparison of the long wavelength response of the cells in the six lots with the observed short circuit distributions of Figure 10 shows a one-to-one correspondence in group order.

TI N⁺/P SOLAR CELL-IE CURVE-5 GRID TI-5958   DRIFT FIELD

RUN NO	CUSTOMER		TYPE				BASE RESISTIVITY	SHEET RESISTANCE
LOT 1-A-4	NASA		1.8	CM.²	5 GRID		Ω —CM.	Ω /SQ.
INTENSITY		TEMP.	DATE	TIME	TEST SITE		TESTER	FILTER
100 MW/CM²TUNGSTEN		28 °C	10/26/65	3 PM	TI		GM DB	3CM H₂O
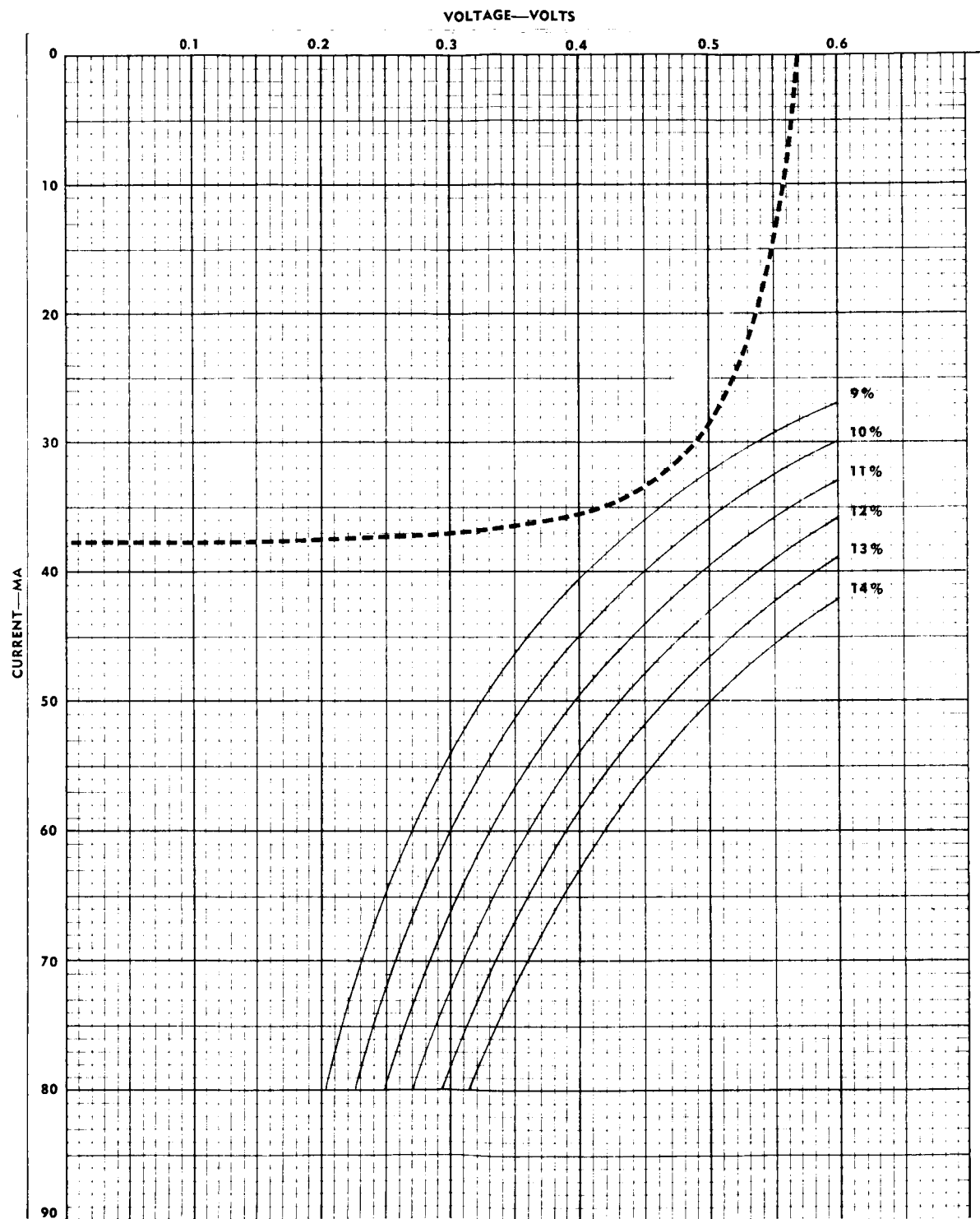
Figure 2.   Solar Cell IE Curve for Cell 1-A-4

SC01942

8

TI N$^+$/P SOLAR CELL-IE CURVE—5 GRID TI-595B   DRIFT FIELD

RUN NO	CUSTOMER		TYPE			BASE RESISTIVITY	SHEET RESISTANCE	
LOT 1-B-2	NASA		1.8	CM.² 5 GRID		Ω —CM.		Ω /SQ.
INTENSITY		TEMP.	DATE	TIME	TEST SITE		TESTER	FILTER
100 MW/CM²TUNGSTEN		28 °C	10/26/65	3 PM	TI		GM DB	3CM H₂O
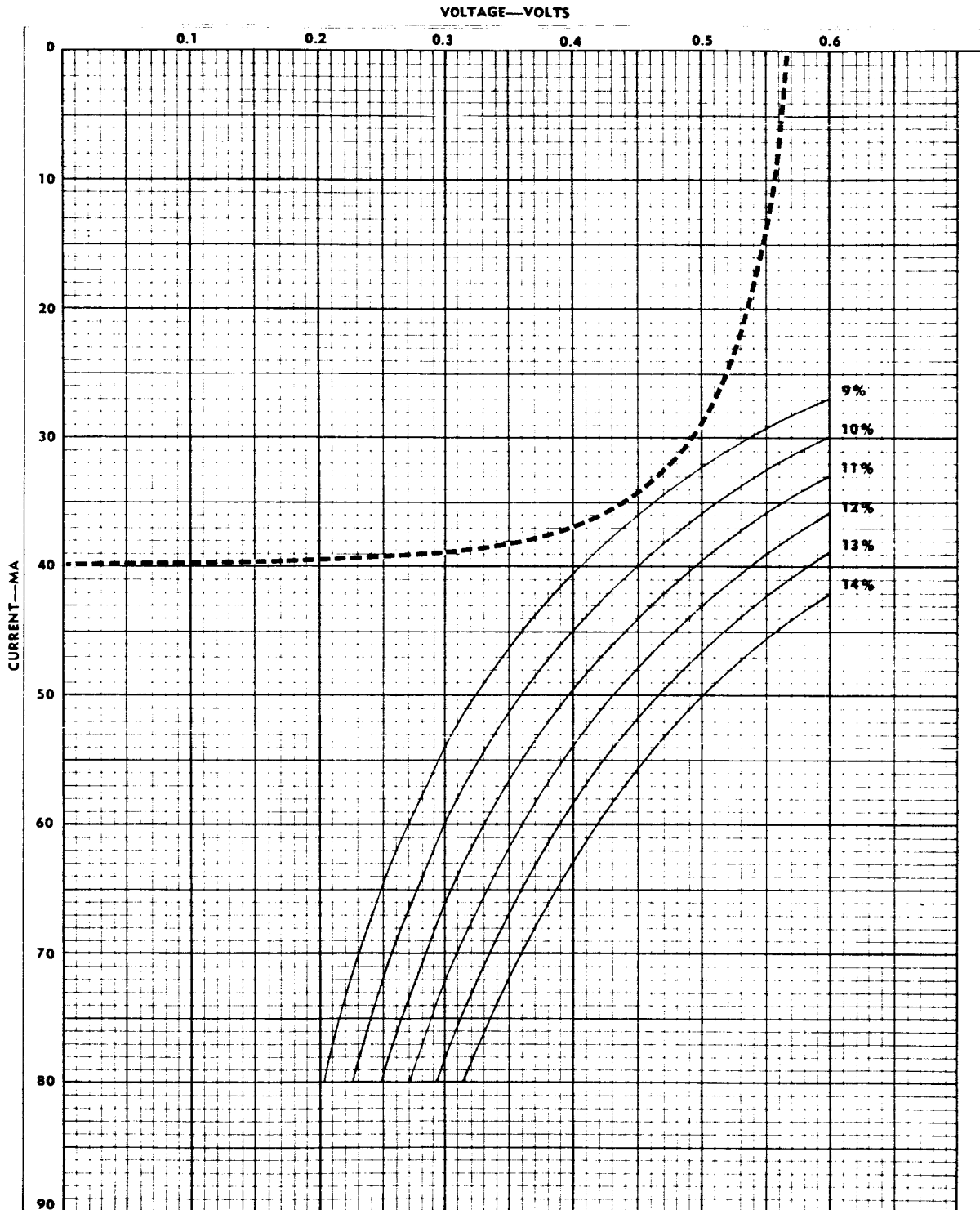
SC01943

Figure 3.   Solar Cell IE Curve for Cell 1-B-2

9

TI N⁺/P SOLAR CELL-IE CURVE – 5 GRID TI-5958   DRIFT FIELD

RUN NO.	CUSTOMER	TYPE			BASE RESISTIVITY	SHEET RESISTANCE
LOT 2–4	NASA	1.8	CM.²	5 GRID	Ω —CM.	Ω /SQ.

| INTENSITY		TEMP.		DATE	TIME	TEST SITE	TESTER	FILTER
100 MW/CM²TUNGSTEN		28 °C		9/14/65	1 PM	TI	G. M.	3CM H₂O
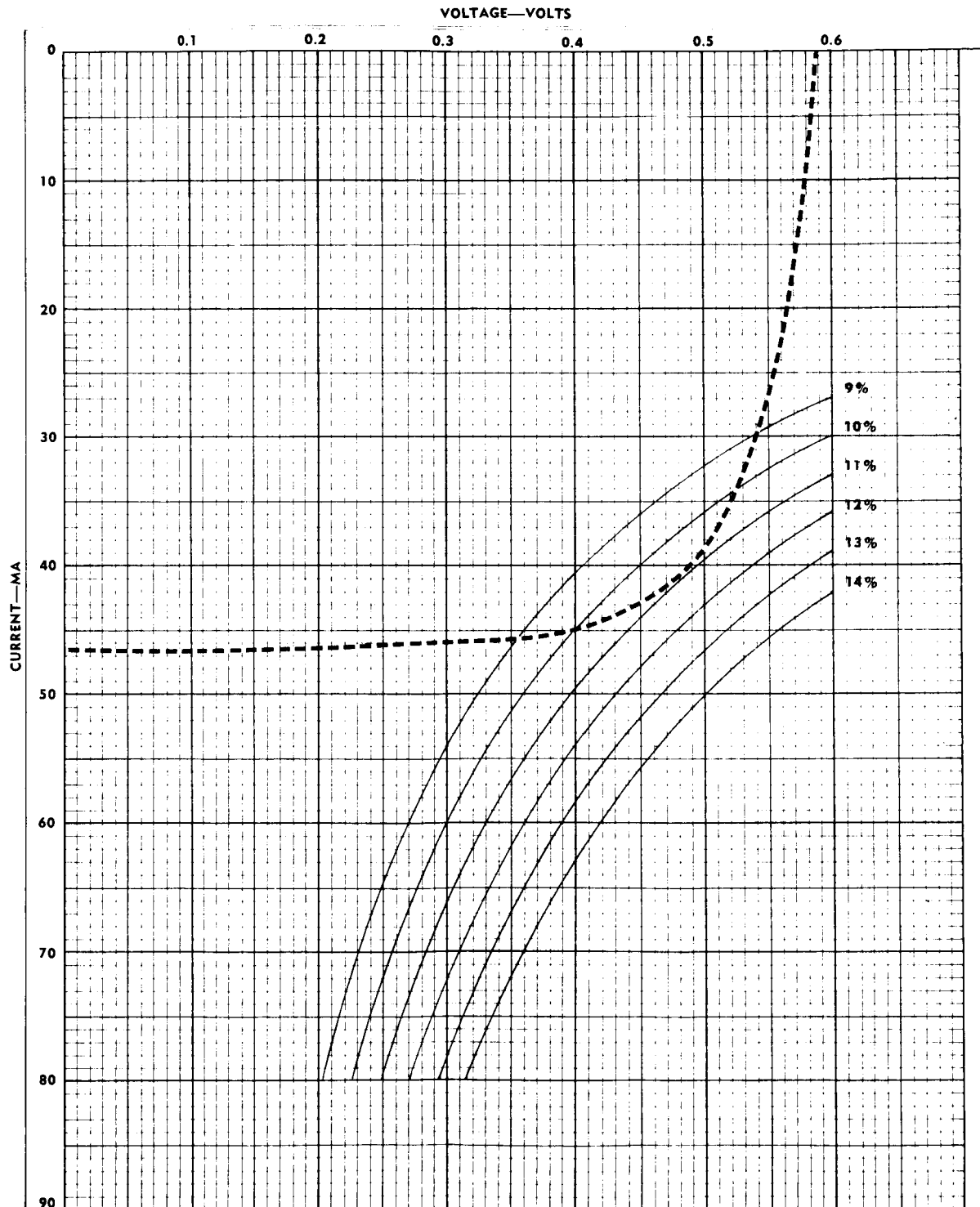
Figure 4.   Solar Cell IE Curve for Cell 2-4

SC01944

10

TI N⁺/P SOLAR CELL-IE CURVE—5 GRID   TI-5958   DRIFT FIELD

RUN NO	CUSTOMER	TYPE			BASE RESISTIVITY	SHEET RESISTANCE
LOT 3-8	NASA	1.8	CM.²	5 GRID	Ω —CM.	Ω /SQ.
INTENSITY		TEMP.	DATE	TIME	TEST SITE	TESTER	FILTER
100 MW/CM²TUNGSTEN		29 °C	8/27/65	4 PM	TI	G. M. — D. B.	3CM H₂O

VOLTAGE—VOLTS
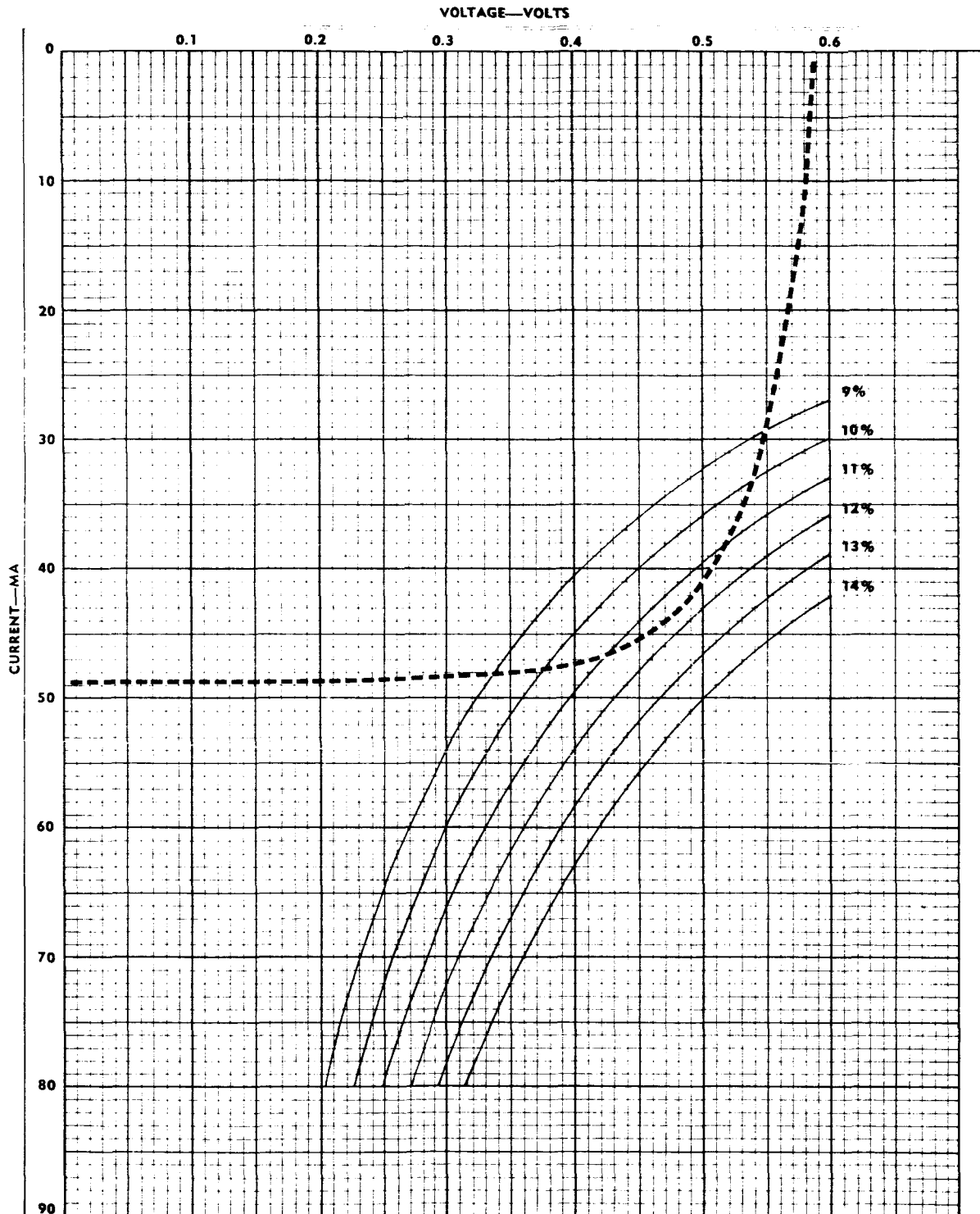
Figure 5.   Solar Cell IE Curve for Cell 3-8

SC01945

11

TI N⁺/P SOLAR CELL-IE CURVE—5 GRID TI-5958   DRIFT FIELD

RUN NO	CUSTOMER	TYPE			BASE RESISTIVITY	SHEET RESISTANCE	
LOT 4-6	NASA	1.8	CM.² 5 GRID		Ω —CM.		Ω /SQ.

INTENSITY	TEMP	DATE	TIME	TEST SITE	TESTER	FILTER
100 MW/CM²TUNGSTEN	29 °C	8/27/65	4 PM	TI	GM DB	3CM H₂O

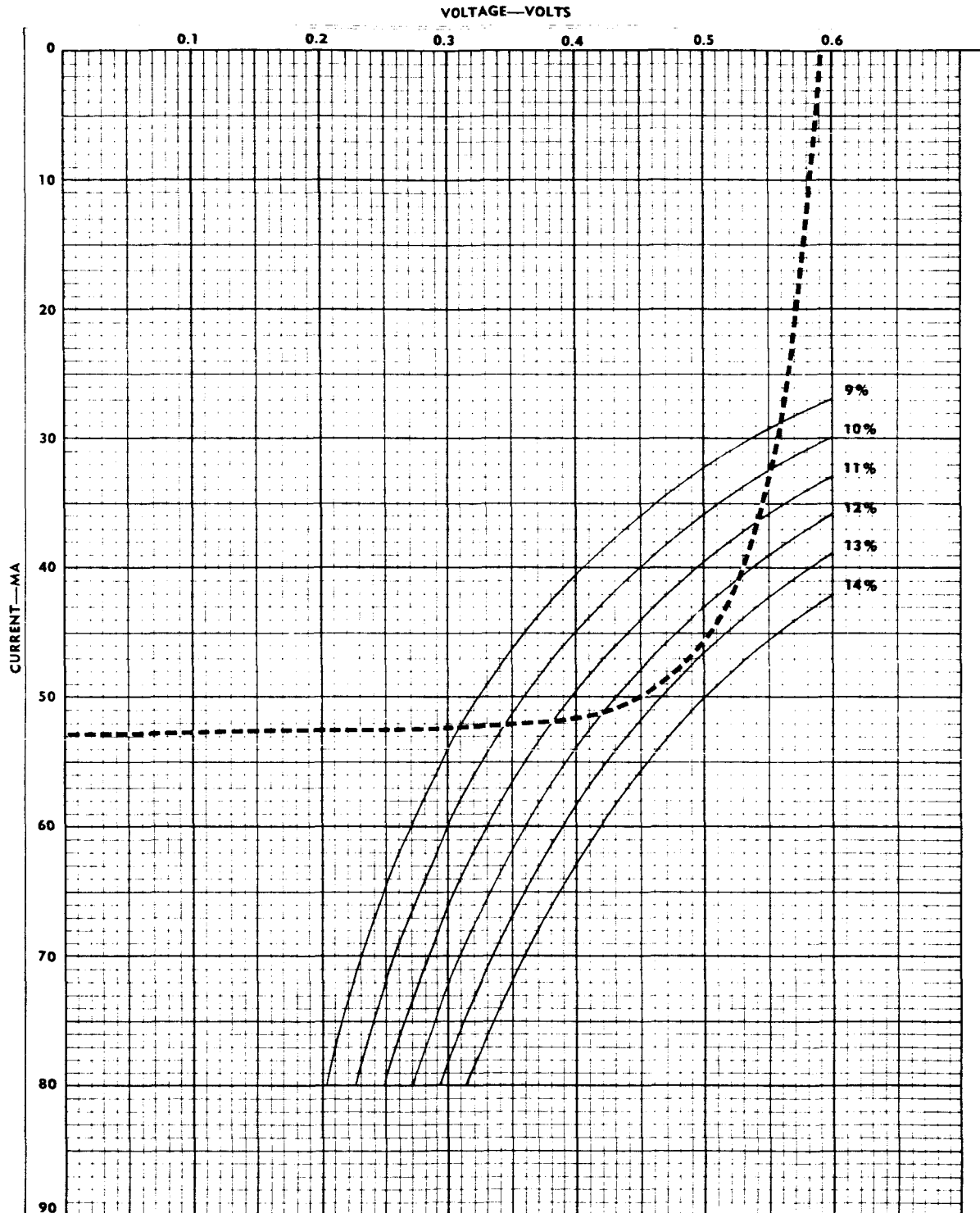VOLTAGE—VOLTS   DRIFT FIELD
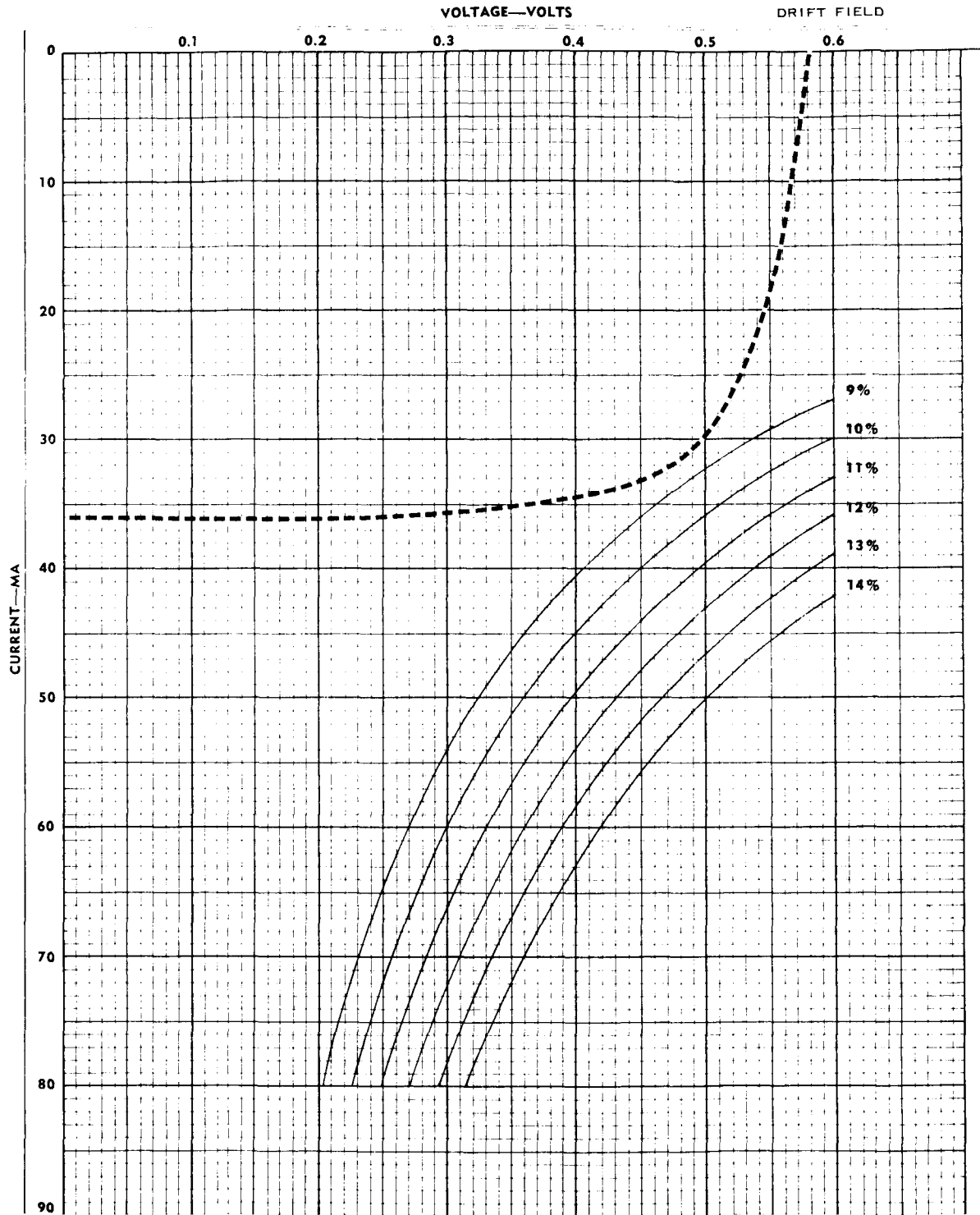
SC01946

Figure 6.   Solar Cell IE Curve for Cell 4-6

TI N⁺/P SOLAR CELL-IE CURVE—5 GRID TI-5956   DRIFT FIELD

RUN NO.	CUSTOMER	TYPE				BASE RESISTIVITY	SHEET RESISTANCE
LOT 5-4	NASA	1.8	CM.²	5 GRID		Ω —CM.	Ω /SQ.
INTENSITY	TEMP.	DATE	TIME	TEST SITE		TESTER	FILTER
100 MW/CM²TUNGSTEN	28 °C	9/14/65	1 PM	TI		G. M.	3CM H₂O

Figure 7.   Solar Cell IE Curve for Cell 5-4
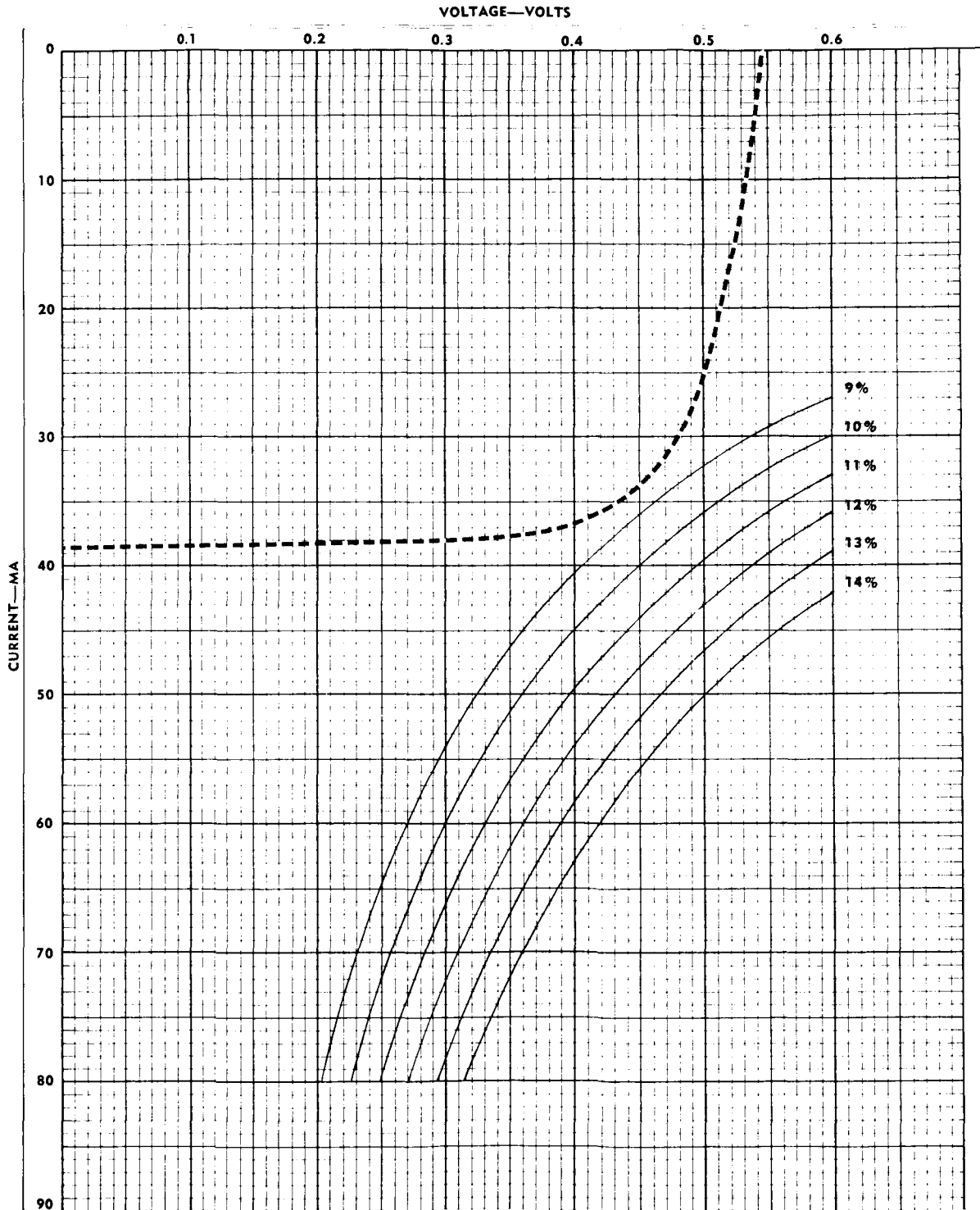
SC01947

Figure 8. Solar Cell IE Curve for Cell 6-A-5

SC01948

TI N⁺/P SOLAR CELL-IE CURVE-5 GRID TI-5958   DRIFT FIELD

RUN NO	CUSTOMER	TYPE		BASE RESISTIVITY	SHEET RESISTANCE
LOT 6-B-5	NASA	1 8 CM.² 5 GRID		Ω —CM.	Ω /SQ.
INTENSITY	TEMP	DATE TIME	TEST SITE	TESTER	FILTER
100 MW/CM²TUNGSTEN	28 °C	10/26/65 3 PM	TI	GM DB	3CM H₂O
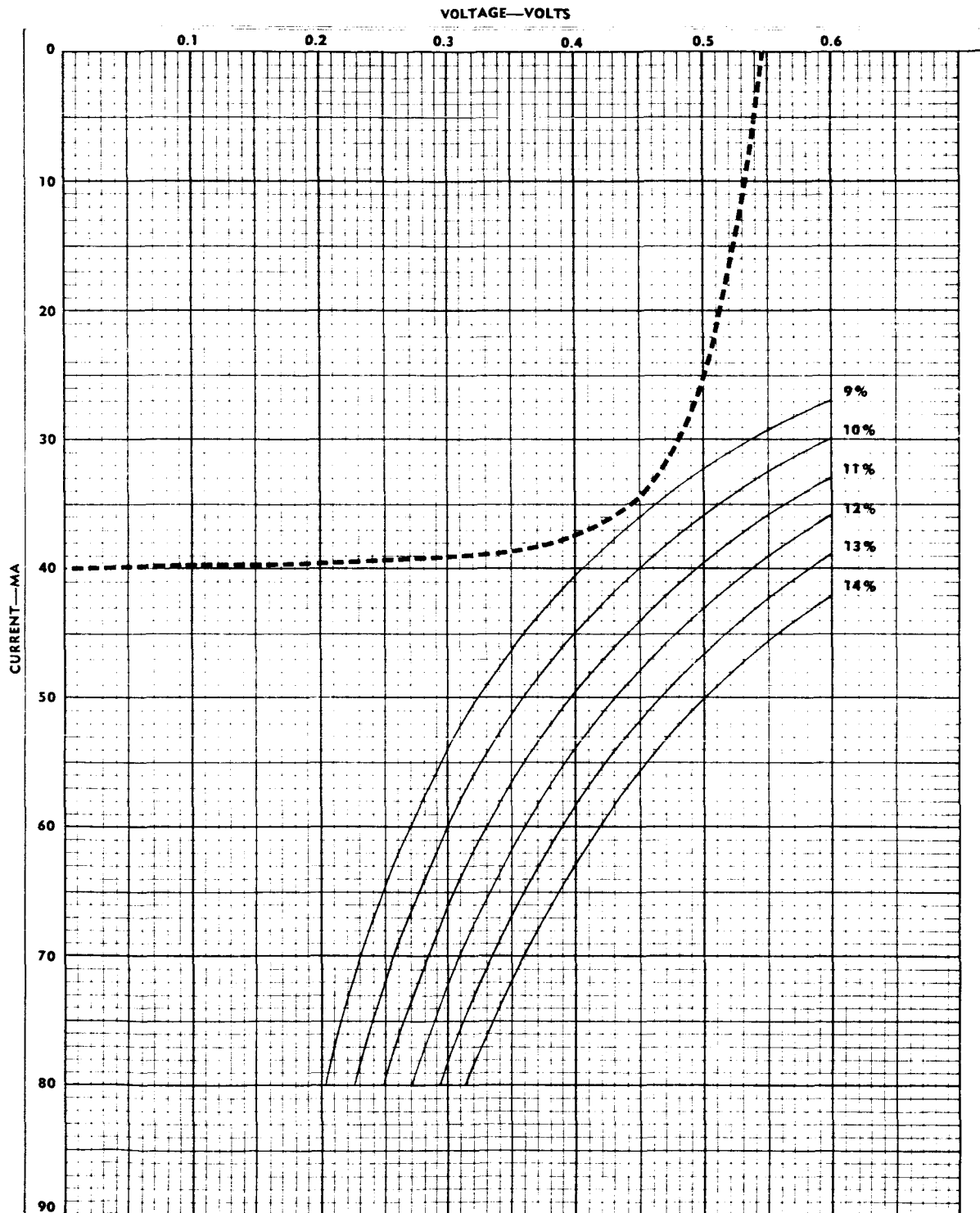
SC01949

Figure 9.   Solar Cell IE Curve for Cell 6-B-5
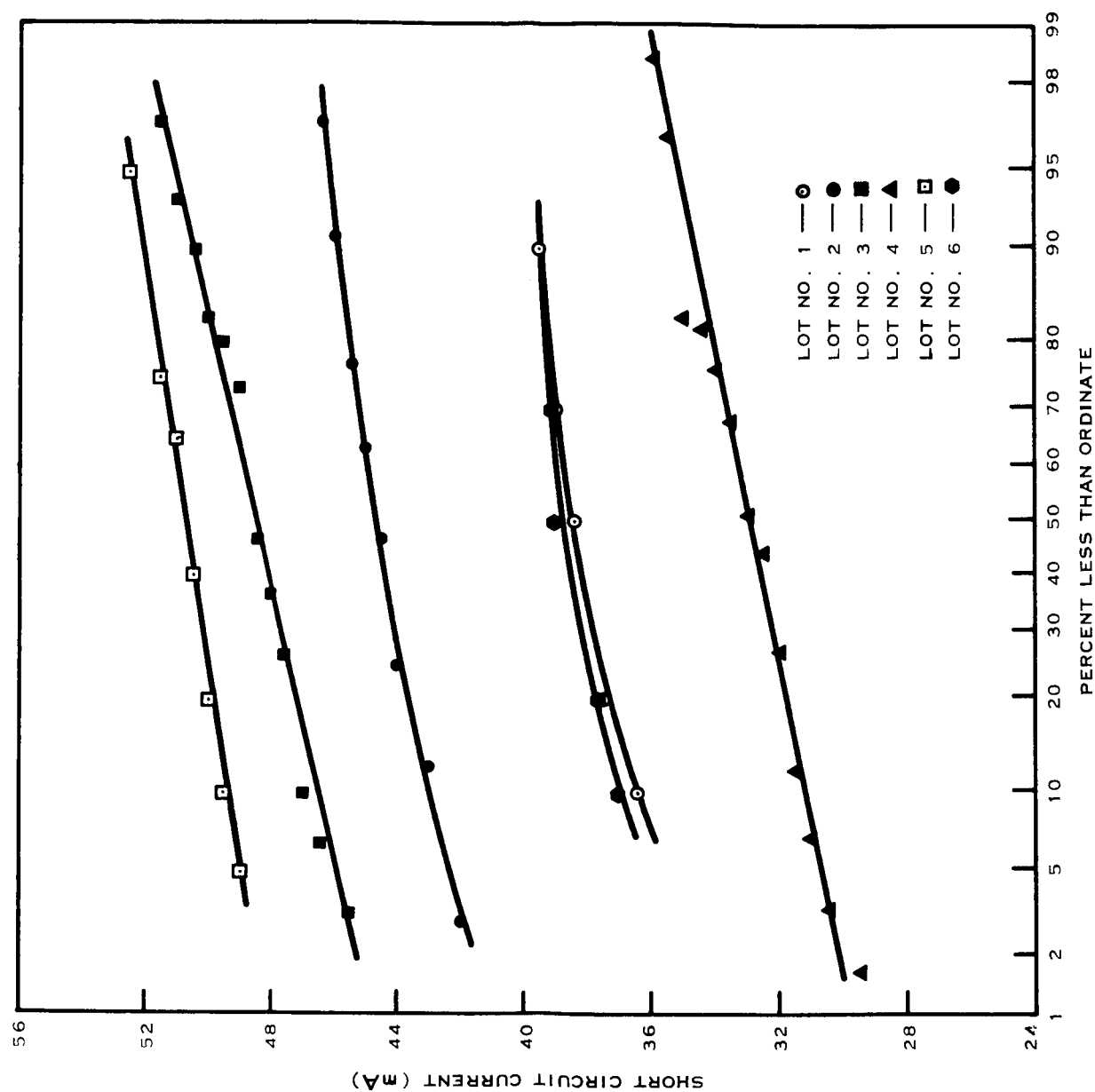
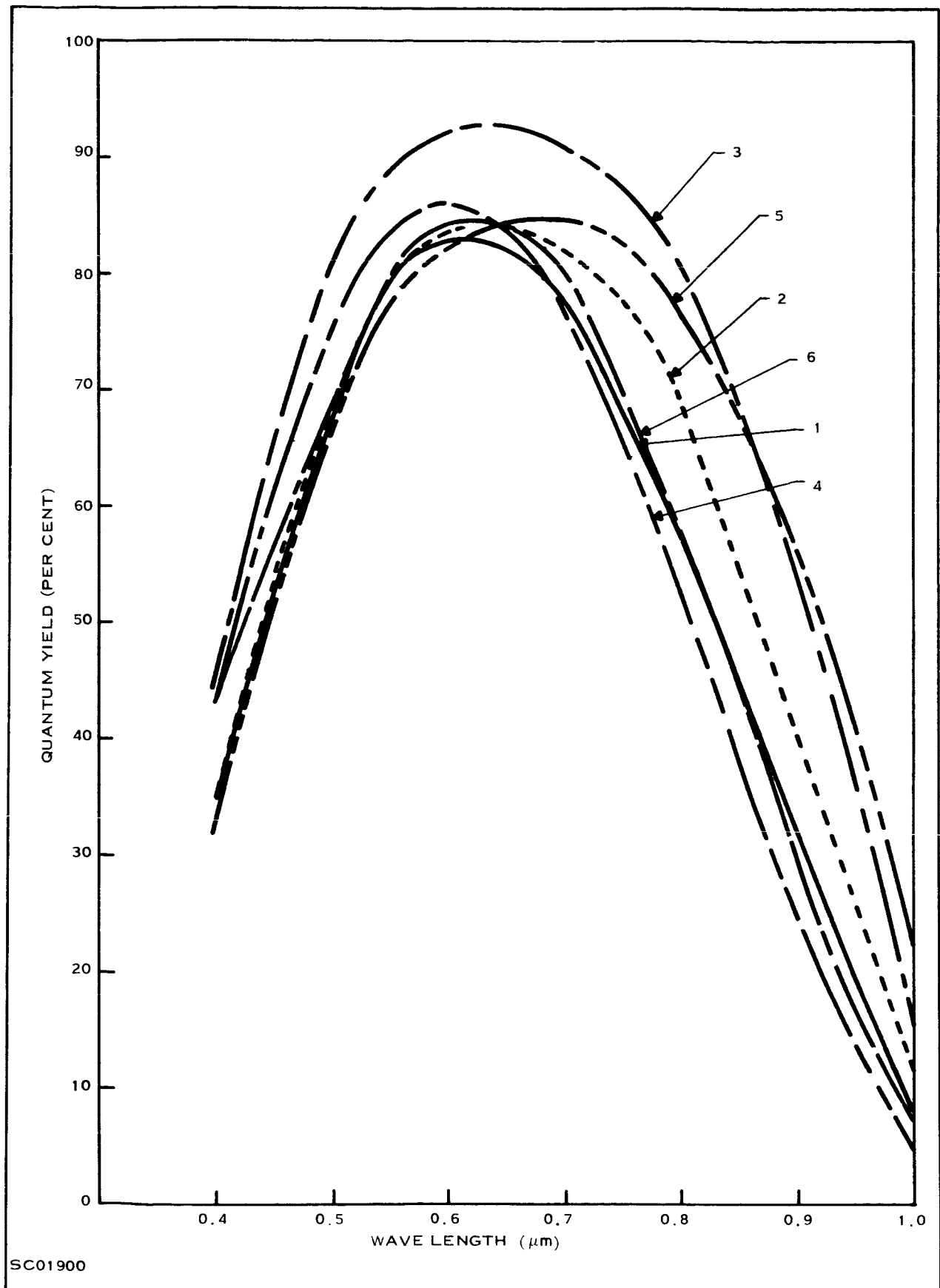Figure 10. Short Circuit Current Distribution (Unirradiated Cells)

SC01899

Figure 11. Wavelength Response before Irradiation

SECTION III

RADIATION RESULTS

A. GENERAL

Radiation experiments were conducted by NASA on cells from the sixty samples submitted by TI. Electron bombardment at a one MeV level was made to a cumulative flux value of 1×10^{16} electrons/cm^2. Current voltage curves were obtained for 100 mW/cm^2 tungsten light illumination after various irradiation periods. Quantum yield data also were obtained after the last period of irradiation. From two to four samples in each group were irradiated. Results within a group were sufficiently close such that average values have been used in plotting the current-voltage characteristics of the irradiated cells.

B. CURRENT-VOLTAGE CHARACTERISTICS OF THE IRRADIATED CELLS

The absolute values of short-circuit current (I_{sc}), open-circuit voltage (V_{oc}), and maximum power density, each as a function of integrated electron flux, are presented in Figures 12 to 17. Although the values of these electrical parameters as measured by NASA for the pre-irradiated cells are generally higher than the values shown in Table II (measured at Texas Instruments Incorporated), the differences apparently are due only to use of different standard cells.

The effect of drift field width (at constant three-order-of-magnitude field) on degradation of I_{sc}, V_{oc}, and maximum power density is shown in Figures 12, 13 and 14. The initial positional order of values of I_{sc} for Lots 1, 2, and 3 is maintained throughout the irradiation, as shown in Figure 12. Positional order of V_{oc} values

19

changes during the irradiation, as shown in Figure 13, but the final voltage values are sufficiently close together that the maximum power density values in Figure 14 have the same order as do the current values in Figure 12.

Figures 15, 16 and 17 display the effect of substrate dopant level and type (at constant 12-micron width field) on degradation of current, voltage, and power. Cells made on the boron-doped substrates (Lots 2, 4, and 5) maintained their initial positional order with respect to current, throughout the irradiation. Samples from cells made on the aluminum-doped substrates (Lot 6) exhibited remarkably low degradation of current. Only 13 percent of the initial value of I_{sc} was lost at an integrated flux of 1×10^{16} electrons/cm^2. On the other hand, the aluminum-doped cells showed the highest percentage degradation in V_{oc}, as shown in Figure 16.

Voltages for cells in Lots 2, 4 and 5 were approximately equal after irradiation. Of the four lots represented in Figure 17, Lot 6 retains the highest maximum power after irradiation. Of the six lots shown in Figures 14 and 17, Lots 3 and 6 have the highest maximum power after irradiation and are approximately equal in value.

The observed degradation of V_{oc} is greatest for the drift-field cells which experience the least degradation of I_{sc}. The calculations shown in Reference [1] were made on the basis of optimizing the short-circuit current from the p-region of the cell. They were not concerned with the effects of degradation of the open-circuit voltage, for which detailed calculations have not been made. Apparently, optimization of I_{sc} is at the expense of V_{oc}.
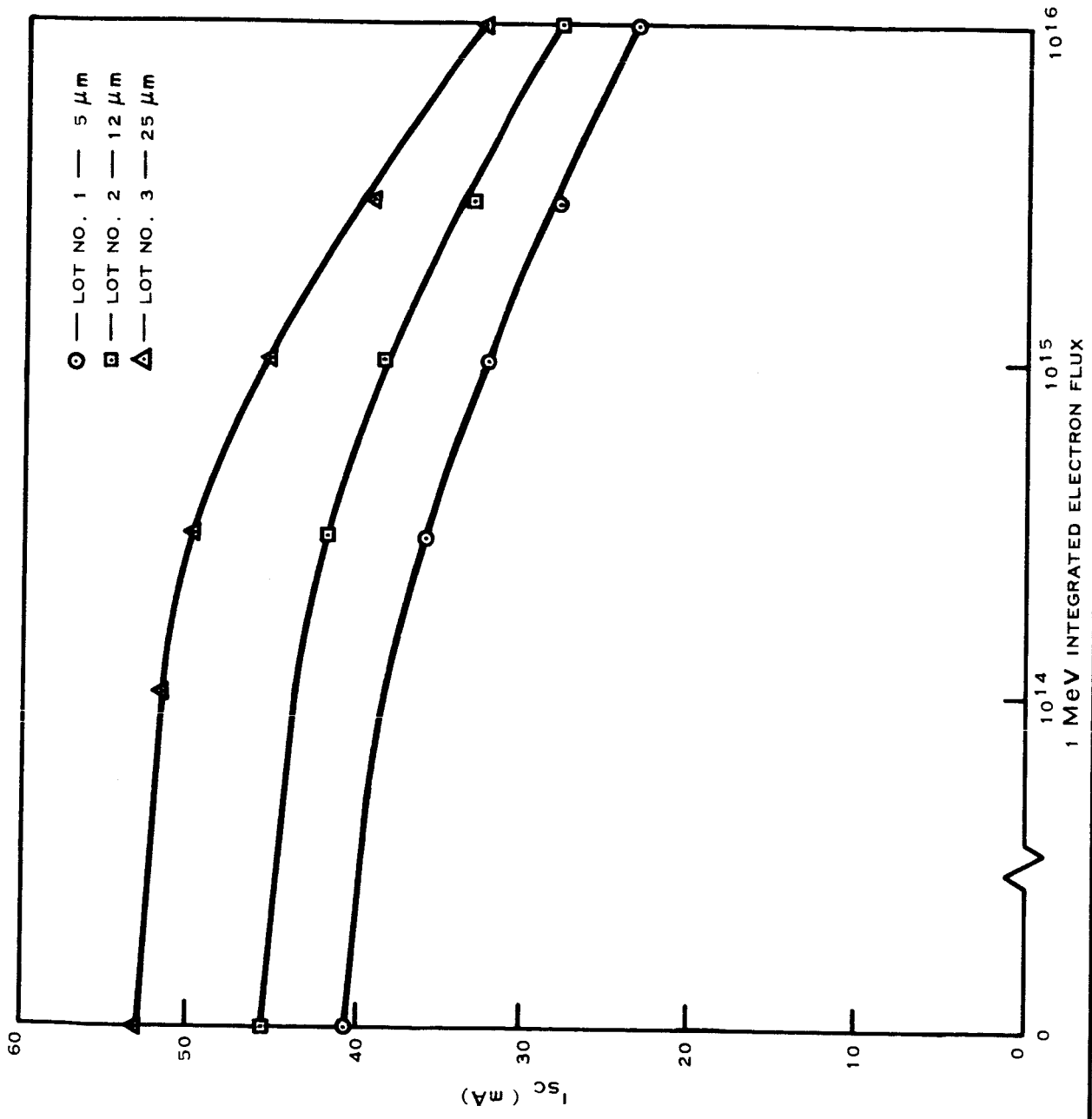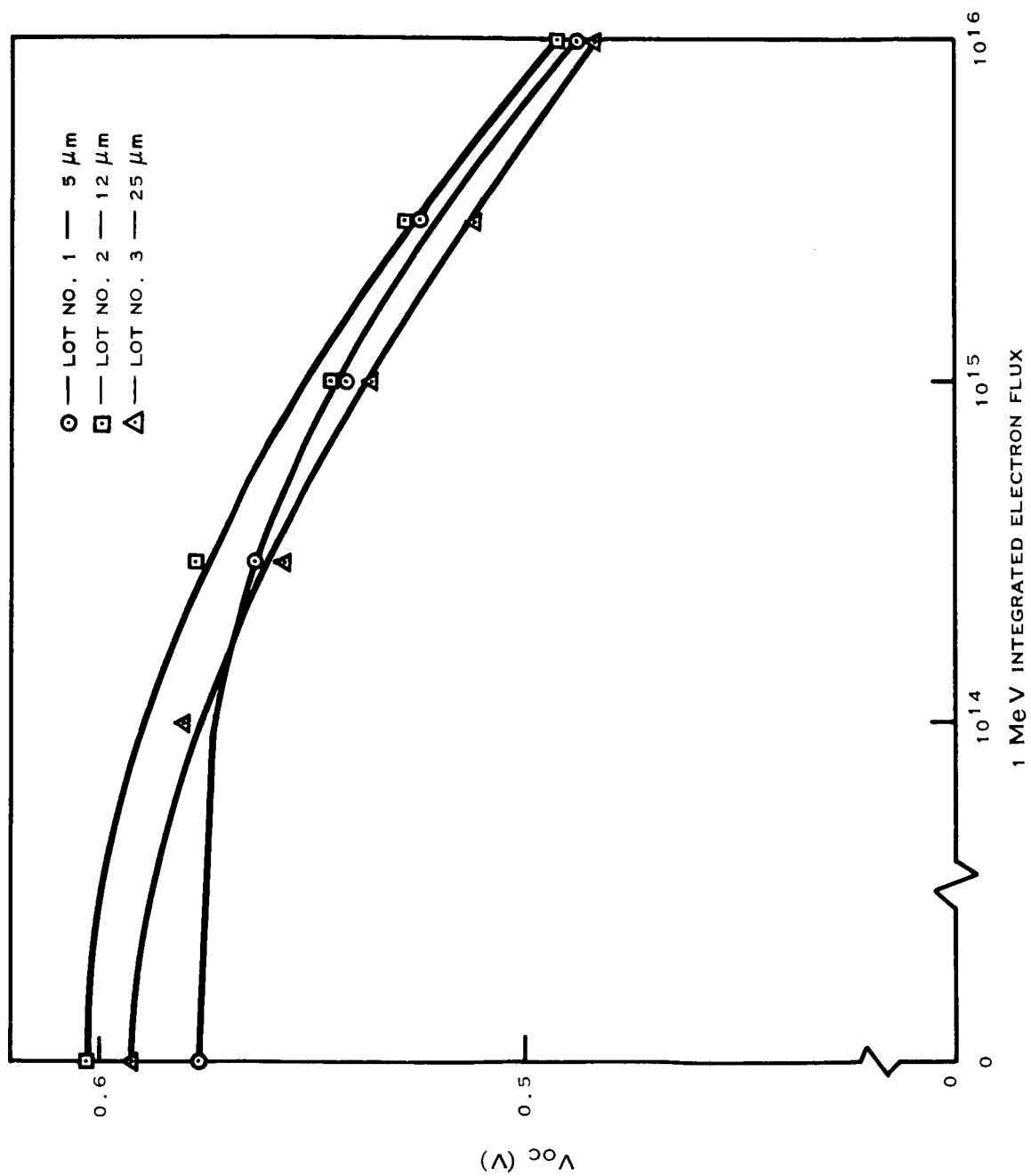
Figure 12.   Effect of Field Width on Current at Constant Three-order-of-magnitude Field

SC01901

Figure 13.   Effect of Field Width on V_{oc} at Constant Three-order-of-magnitude Field
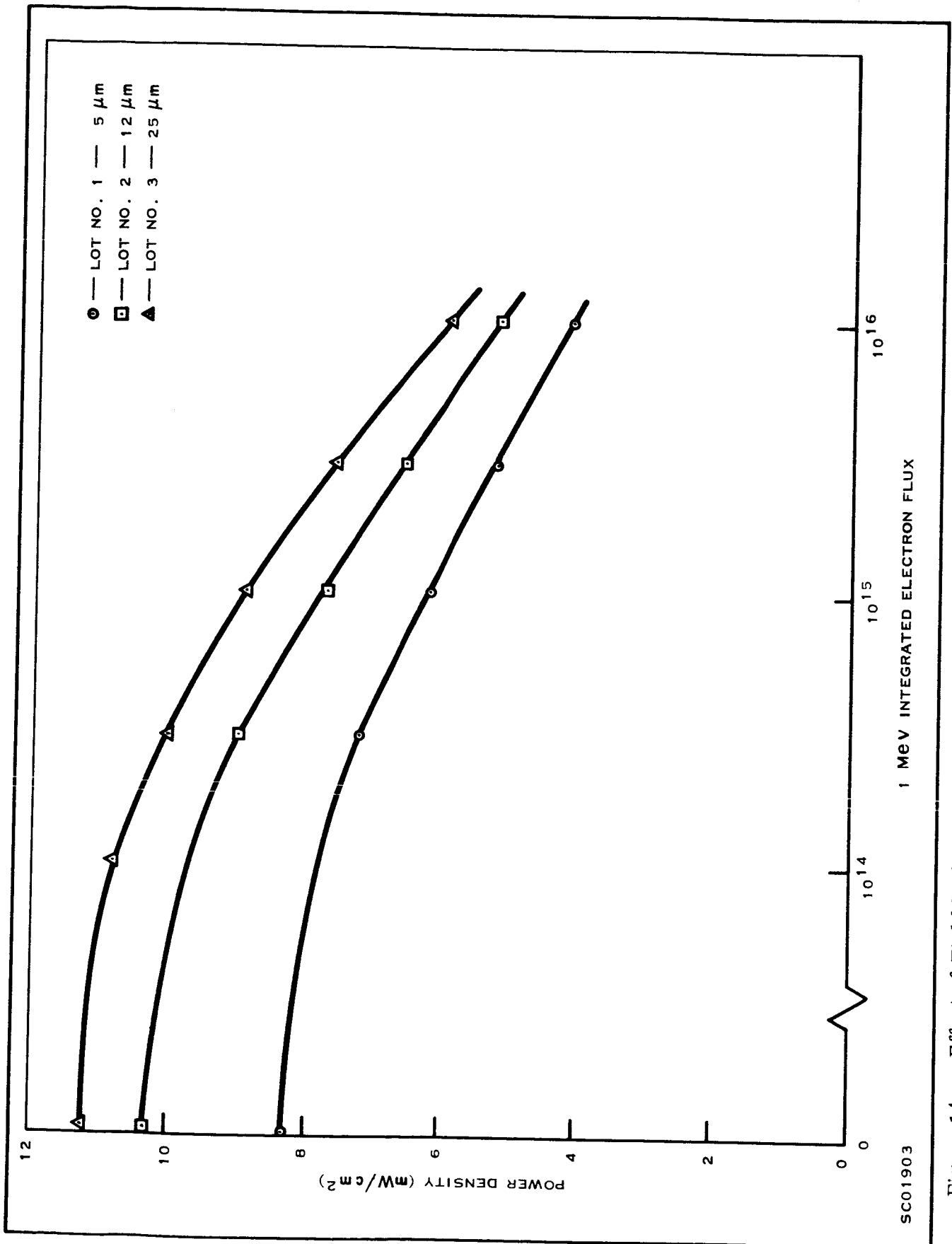
SC01902

Figure 14. Effect of Field Width on Maximum Power Density at Constant Three-order-of-magnitude Field
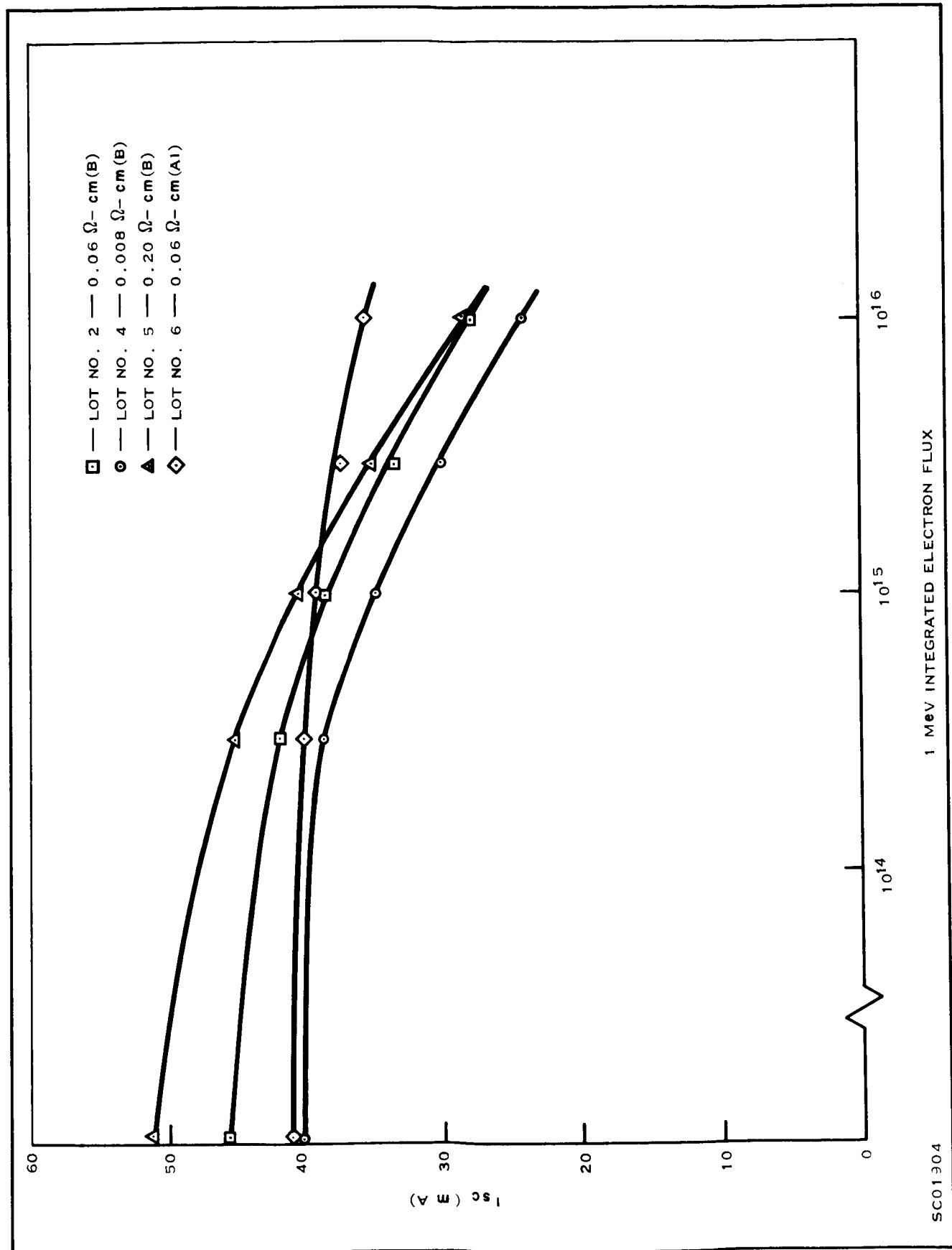
SC01903

Figure 15. Effect of Substrate Dopant Level and Dopant Type on Current (Field Width Constant at 12 Microns)
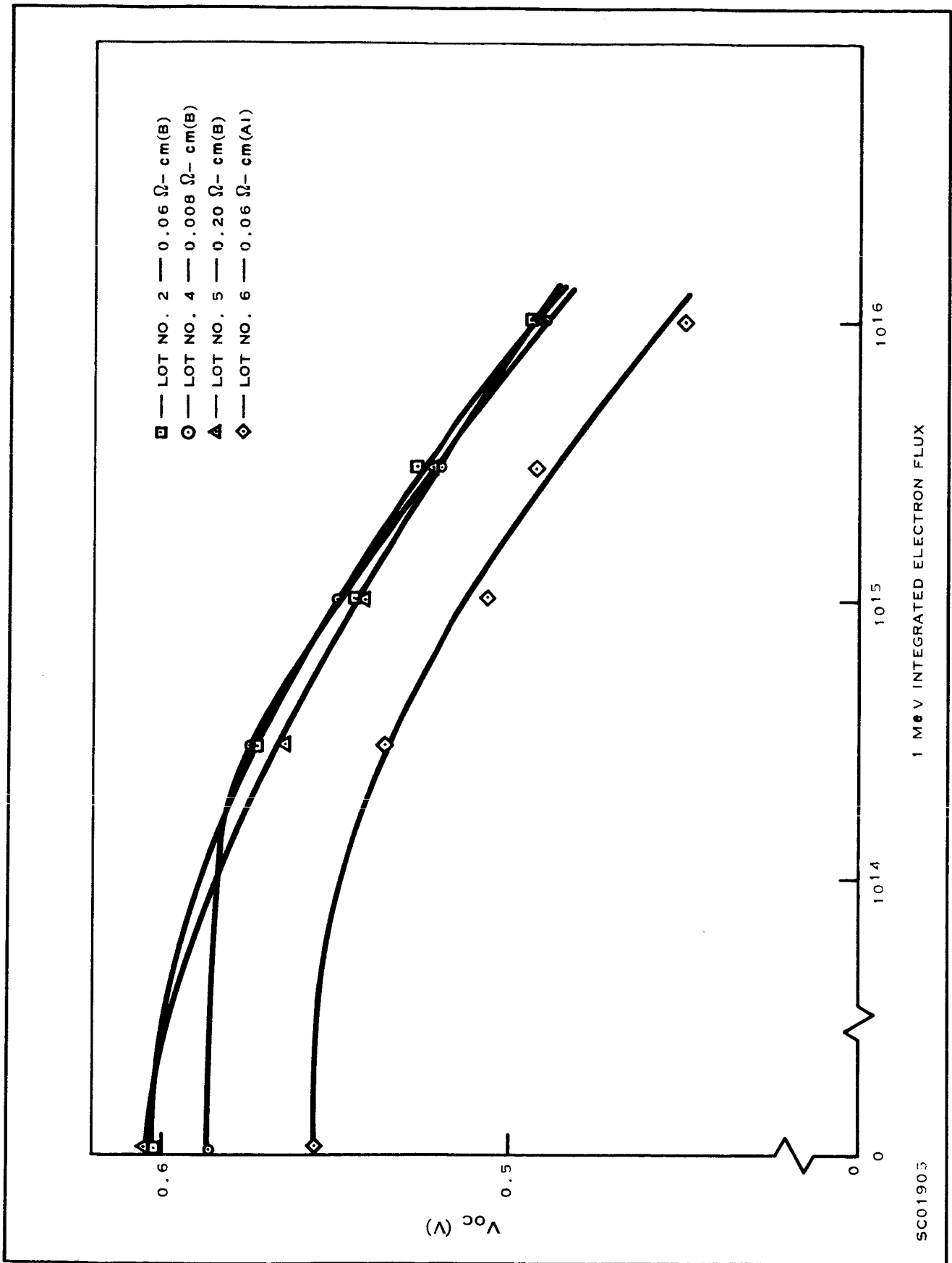
Figure 16.   Effect of Substrate Dopant Level and Dopant
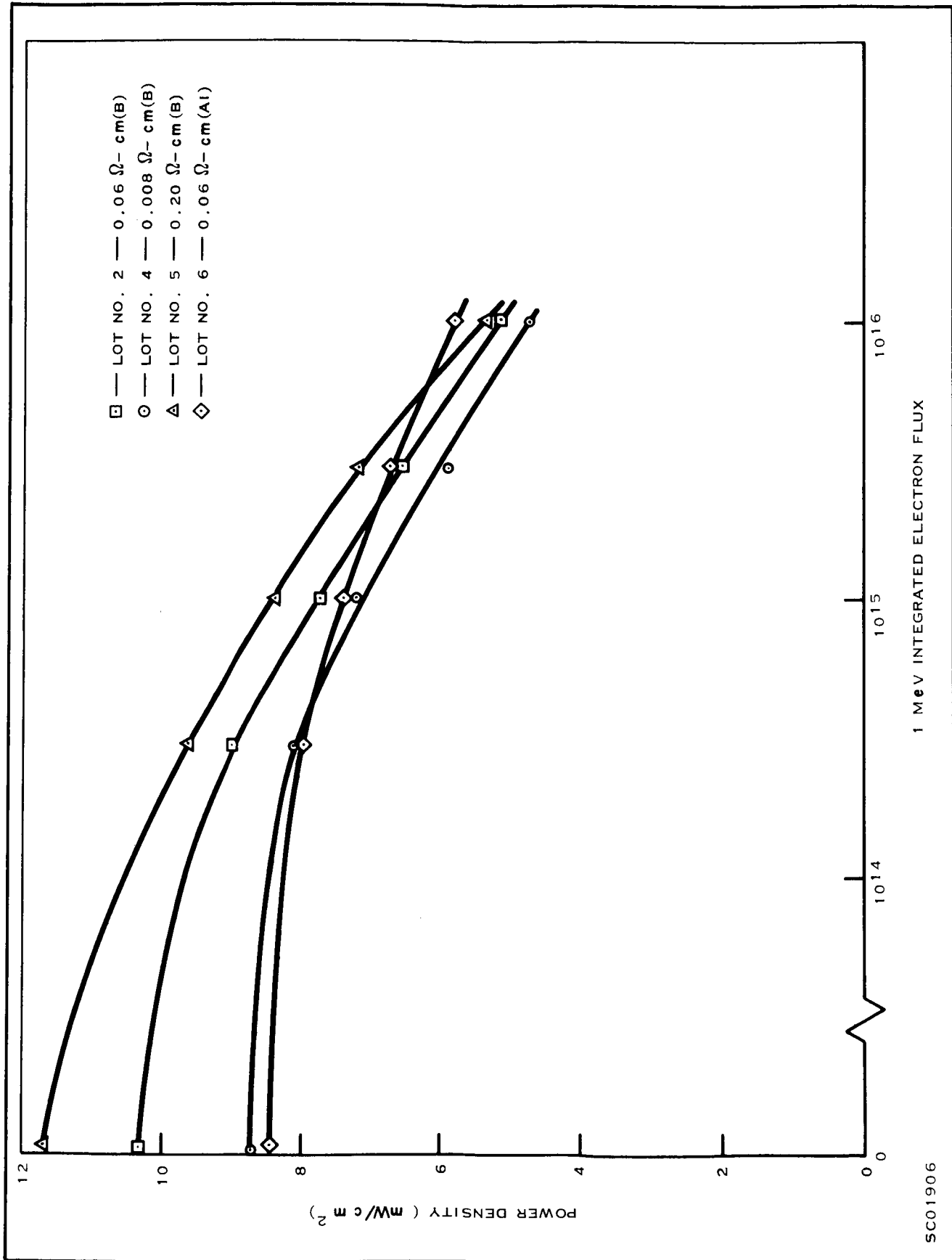Type on Open Circuit Voltage (Field Width Constant at 12 Microns)

Figure 17. Effect of Substrate Dopant Level and Dopant Type on Maximum Power Density (Field Width Constant at 12 Microns)

SC01906

C.   QUANTUM YIELD MEASUREMENTS AFTER IRRADIATION

Quantum yield measurements paralleling those shown in Figure 11 were made on cells from the six lots after they had been irradiated to a cumulative flux of 1×10^{16} electrons/cm^2 at a one MeV level. Results are shown in Figure 18. Once again, a correlation in group order between long-wavelength response and short-circuit current (Figures 12 and 15) is observed. Lot 6, for which the current degradation was low, showed the lowest decrease in long-wavelength response upon irradiation. On the basis of spectral response-lifetime relations [2] these cells apparently had low initial values of lifetime and consequently degraded relatively less with irradiation.

---

[2]   Brian Dale and F. P. Smith, "Spectral Response of Solar Cells," J. Appl. Phys. 32, 1377-81 (1961).
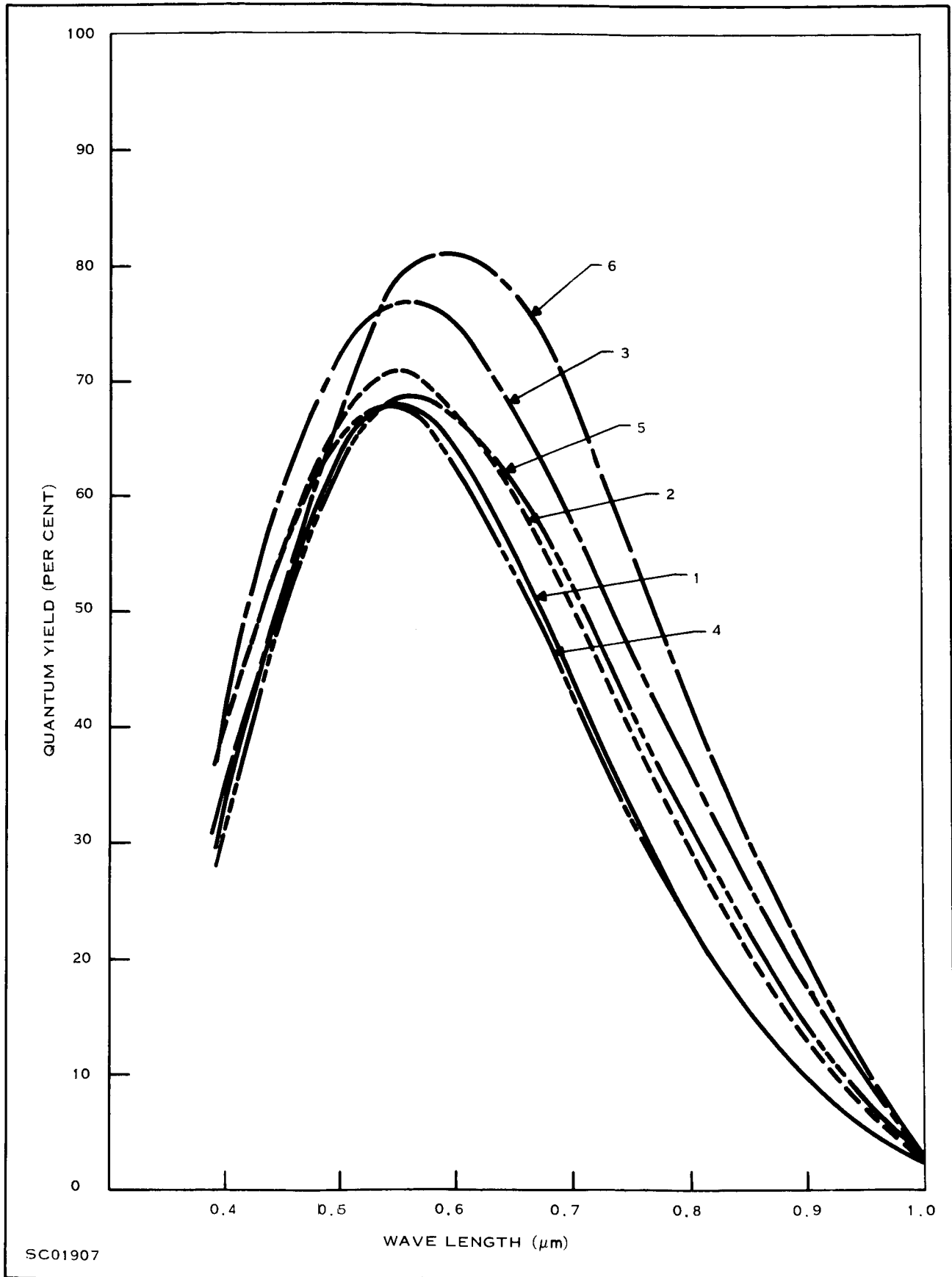
Figure 18. Wavelength Response after 10^{16} 1 MeV Electrons

SC01907

SECTION IV

DISCUSSION OF RESULTS

As was mentioned earlier, the relative behavior of the various cell groups before irradiation quite closely follows previously developed theory for drift-field cells. After irradiation, however, this is no longer true, and in fact, as will be shown, most cells behave as if they had no field. It is true that the predicted improvements for total flux of $10^{16}/cm^2$ are small, and that the varying quality of cells sometimes makes interpretation difficult, but the present data appear to be quite clear.

In order to outline the expected behavior, consider first. Figures 19 and 20, which show calculated short-circuit electron and hole currents versus flux for various widths of fields, and for no field. These two sets of curves may be combined to give total short-circuit current versus flux. The appropriate value for hole current is not clear, since the surface recombination velocity is not known, but if a medium value of 6.2 mA/cm^2 is chosen, then the short-circuit current for no built-in field is plotted in Figure 21 as the solid dots. The relative behavior of short-circuit current for various field widths (assuming a constant three-order-of-magnitude impurity concentration difference) is shown in Figure 22. This illustrates that for fluxes of less than $10^{16}/cm$, there is little difference between the 5-, 12-, and 25-micron fields, though in absolute magnitude there are rather large differences. Since the relative behavior of the three fields is similar, the short-circuit current of only one of these, that for a 12-micron width versus flux, was normalized to the no-field case and also plotted on Figure 21 as the solid squares. Now, if all of the data for TI Lots 1, 2, 3, 4 and 5, along with that from one non-drift-field Hoffman and one non-drift-field RCA cell are normalized to the same 55 mA total current and plotted on Figure 21, all of the points fall in the

shaded portion of the curve and are in remarkable agreement with the theoretical non-drift-field case. As a reminder, Lot 1 had a 5 μm field, Lot 2 a 12 μm field, Lot 3 a 25 μm field (each three orders), Lot 4 a 12 μm, four-order field and Lot 5 a 12 μm, two-order field. Yet all of these cells, when normalized, grouped within ± 4 percent of each other and were quite close to values predicted for no field.

In order to examine these data in another manner, the values of short-circuit current after $10^{16}/cm^2$, along with calculated values and an experimental value for a Westinghouse drift-field cell, [3] were plotted bar chart style. This is shown in Figure 23, from which it can again be clearly seen that not only does the field not enhance cell performance, but because of poor initial values, they are generally inferior. On the basis of these data, one is led to the following alternates:

1) The data are not accurate enough to warrant drawing any conclusions.

2) The theory predicting enhancement is in error.

3) No drift field was actually built in.

4) Irradiation removed the field.

5) Irradiation produced some effect which counteracted the field.

There are some instances (to be considered later) in which the data are suspect, but for the sets that were chosen (all but one of the groups which were manufactured under this contract, and a number of cells which were from the previous contract), the close grouping and remarkable similarity of behavior lend confidence to these data.

---

[3] K. S. Tarneja, F. G. Ernick, and W. R. Harding, "Drift Field Structures Using Epitaxial Growth," presented at the Electrochemical Society Meeting, San Francisco, May 1965.

The theory seems quite in order, though the choice of a K value ($\frac{1}{\tau} = \frac{1}{\tau_0} + K\theta$) that is independent of doping level appears to be a weakness. Also, it has been suggested [4] that one of the terms in the continuity equation has the same sign as the recombination term and behaves mathematically as if the lifetime were reduced. Approximate calculations for one specific case showed no significant difference, but this possibility cannot be ruled out at the present time.

Because of the manner in which the drift-field impurity gradient was introduced, the well ordered pre-irradiation behavior of the various sets, and the results of the cells actually profiled, there is no doubt about the presence of the field.

It is conceivable that the irradiation produces active centers which in turn increase the resistivity in the original drift region and gradually eliminates the field. Such an effect is known to exist,[5] but it seems too small to affect the fields in question. There are some data, however, which indicate that the constant which relates lifetime to total flux is radically dependent on the impurity-concentration[5,6]. Some of these data are shown in Figure 24. By making use of these variations, the electron current for case 4 of Figure 19 (i.e., the 12 micron wide, 3 order-of-magnitude drift field) was recomputed and is shown as curve 6 of Figure 19. The effect of this variable K is to reduce the possible enhancement due to the field. The normalized short circuit computed for the variable K as linearly extrapolated in Figure 24 is represented in Figure 21 by the solid triangles for the 12 micron drift field. As can be seen, the

---

[4]   G. C. Jain and R. M. S. Al-Rifai, "The Effect of Electrostatic-Field-Gradient in Semiconductors with Diffused Impurities," to be published.

[5]   N. Almeleh, B. Goldstein, and J. J. Wysocki, Radio Corporation of America, "Radiation Damage in Silicon," Final Report, dated October 1964, Contract No. NAS 5-3788.

[6]   J. Mandelkorn, L. Schwartz, J. Broder, H. Kautz, and R. Ulman, "Effects of Impurities on Radiation Damage of Silicon Solar Cells," J. Appl. Phys. 35, 2258-60 (1964).

magnitude of the change in K reduces considerably the enhancement due to the field. Indeed, selection of a non-linear extrapolation of K to the high doping levels might yield K values capable of producing enough additional lifetime degradation in the concentration-gradient region of the cell to completely negate the effect of the field introduced by the gradient.

Cells in Lot 6, aluminum doped, were considerably different in behavior from the others, as can be seen from Figure 15. In fact, at first glance, this lot appears to follow theory quite nicely, but both its initial short-circuit current and open-circuit voltage are lower than comparable boron runs. It is probable then that the initial lifetime in the aluminum doped cells was considerably lower than in the others, so that irradiation would initially have much less effect on them than on the others. It should be remembered though, that the absolute value at the 10^{16} e/cm^2 flux level is somewhat higher than observed for most of the other cells. An occasional cell in this and the previous contract would show unusually high retention of current after irradiation. For example, cell TI-28 retained more current after irradiation than did cells in Lot 6 (see Figure 25). The aluminum-doped silicon material from which Lot 6 was prepared had more dislocations than did the comparable, boron-doped Lot 2. Whether this has any bearing on the current problem is uncertain, and because of the small amount of data, any conclusion drawn would be highly speculative.
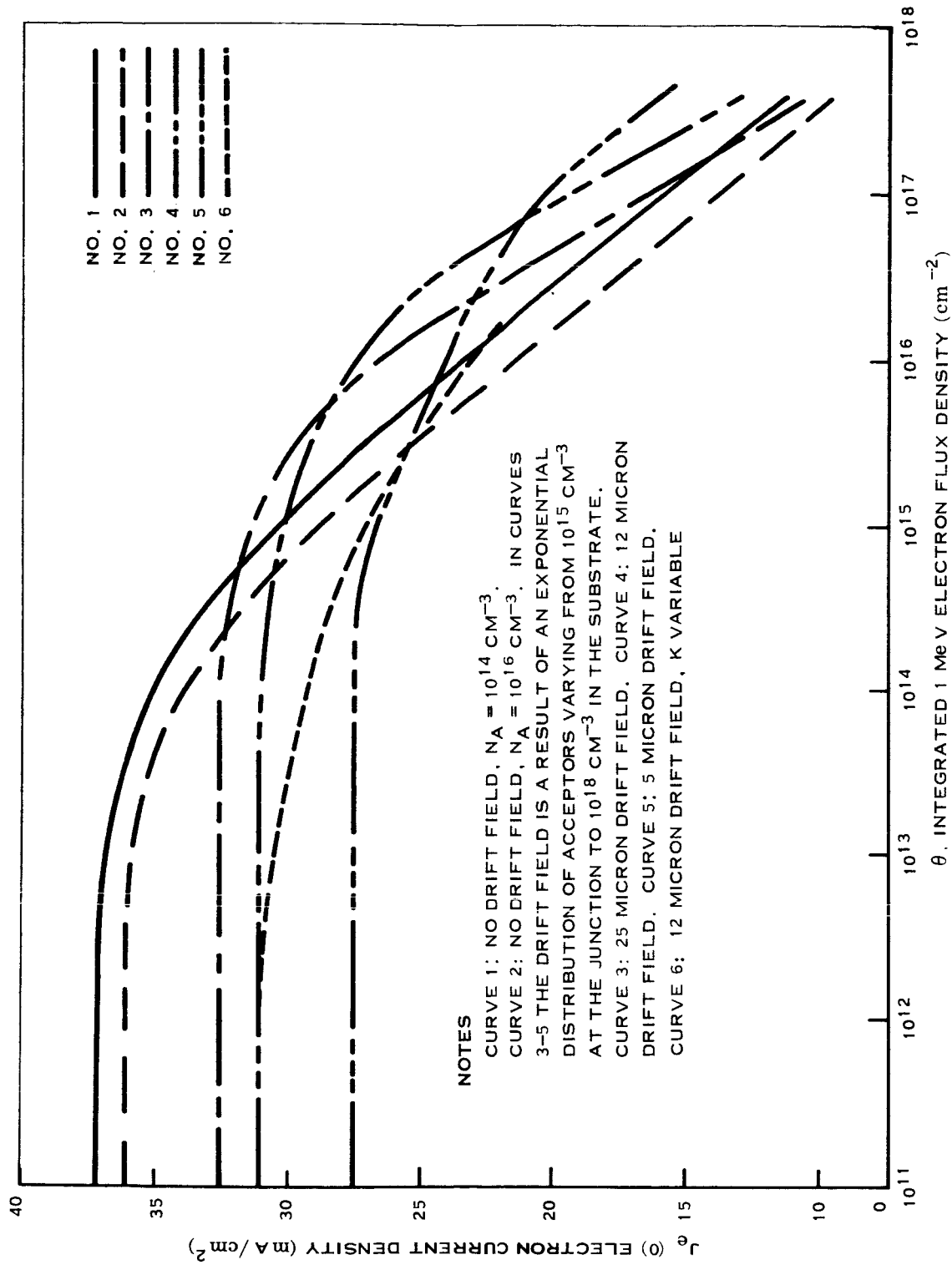
Figure 19.   Effect of Irradiation by 1 MeV Electrons on the Short Circuit Electron Current of an N-on-P Silicon Solar Cell
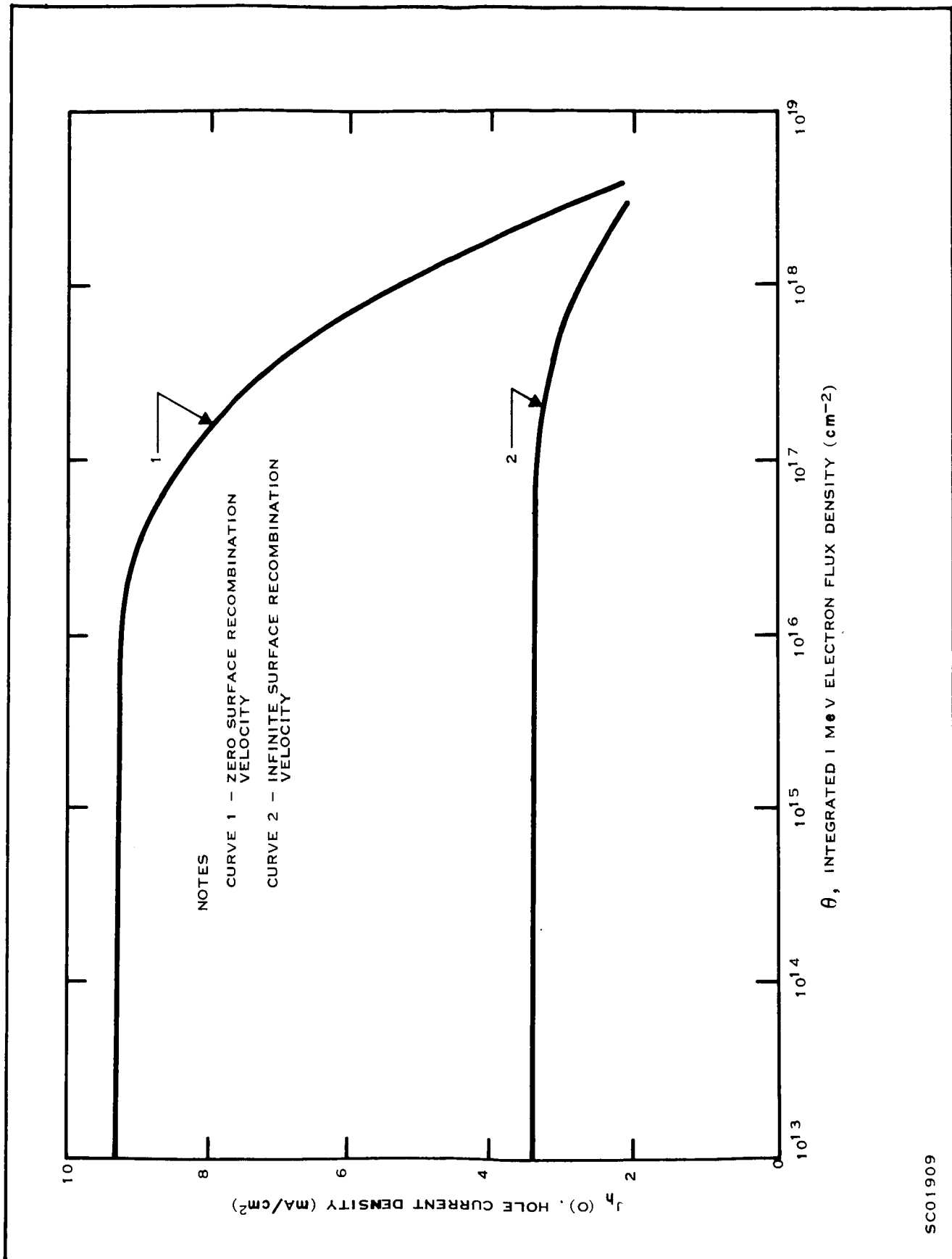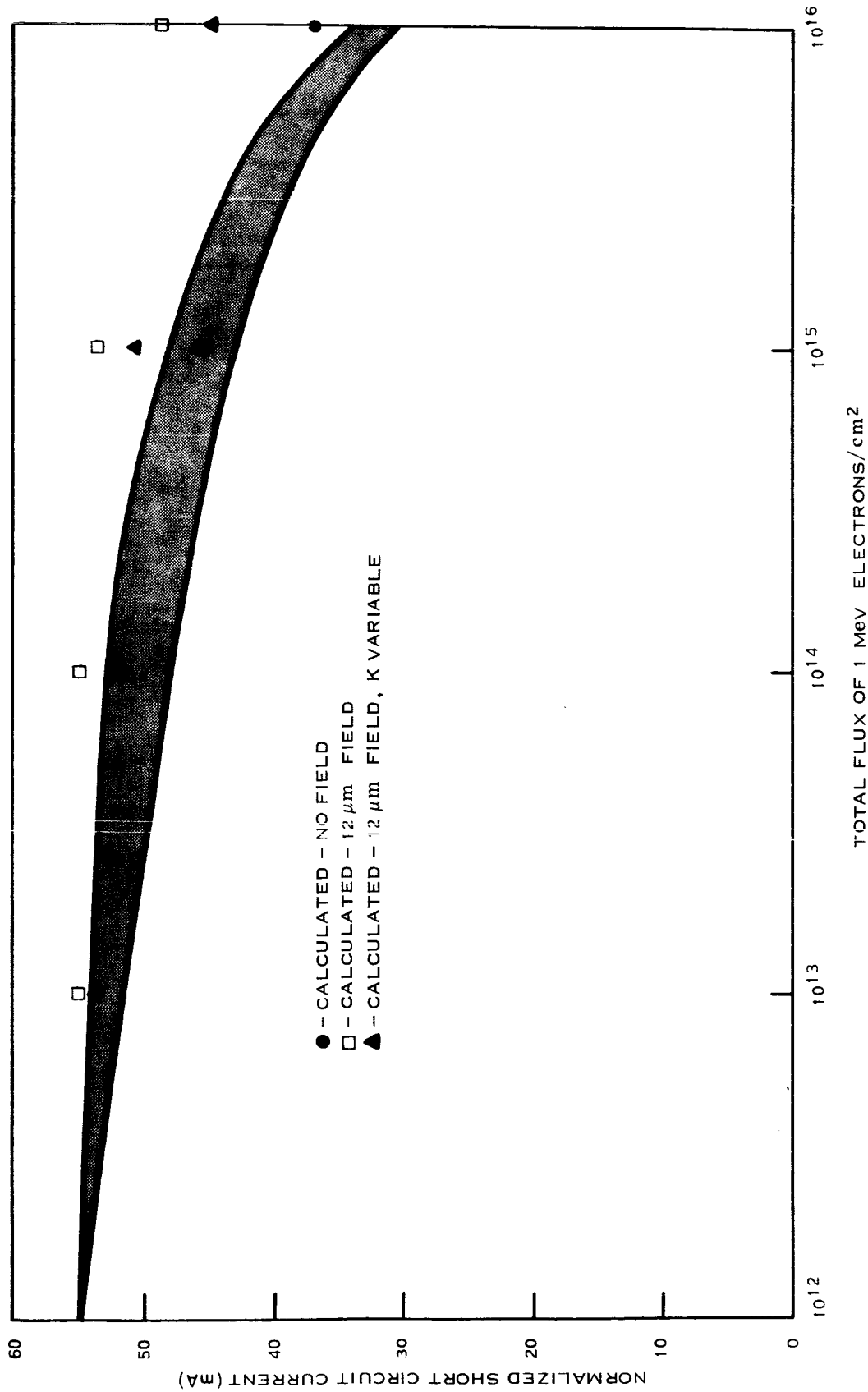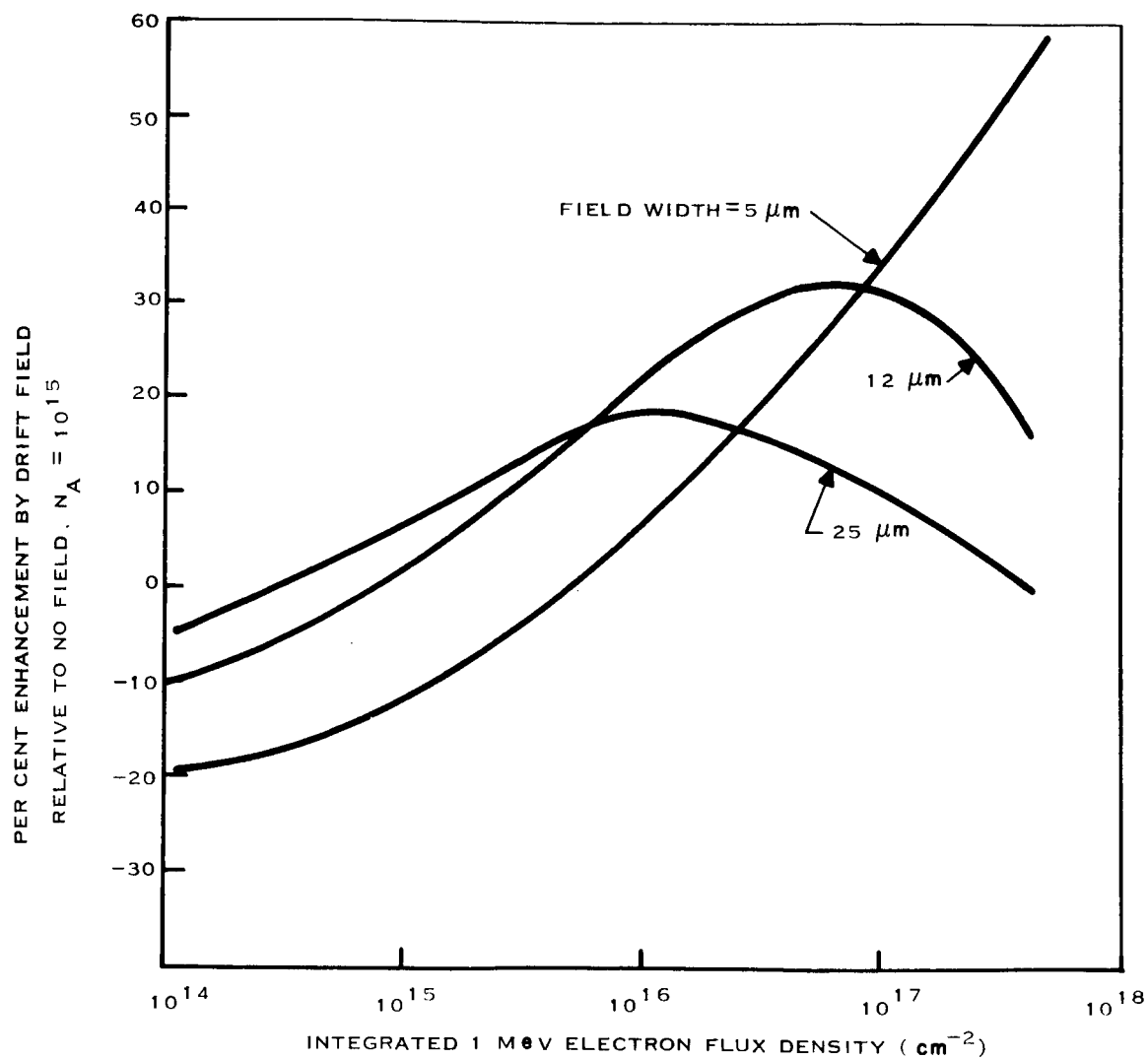
SC01908

Figure 20. Effect of Irradiation by 1 MeV Electrons on the Short Circuit Hole Current of an N-on-P Silicon Solar Cell Having a Diffusion Depth of 0.3 Microns

SC01909

Figure 21. Normalized Current Degradation, Calculated and Experimental

SC01910

● – CALCULATED – NO FIELD
☐ – CALCULATED – 12 μm FIELD
▲ – CALCULATED – 12 μm FIELD, K VARIABLE

TOTAL FLUX OF 1 MeV ELECTRONS/cm²

NORMALIZED SHORT CIRCUIT CURRENT (mA)

Figure 22. Theoretical Percent Enhancement in Short Circuit Current, as a Function of Total Flux, for Three-order-of-magnitude Fields and Field Widths of 5, 12, and 25 Microns
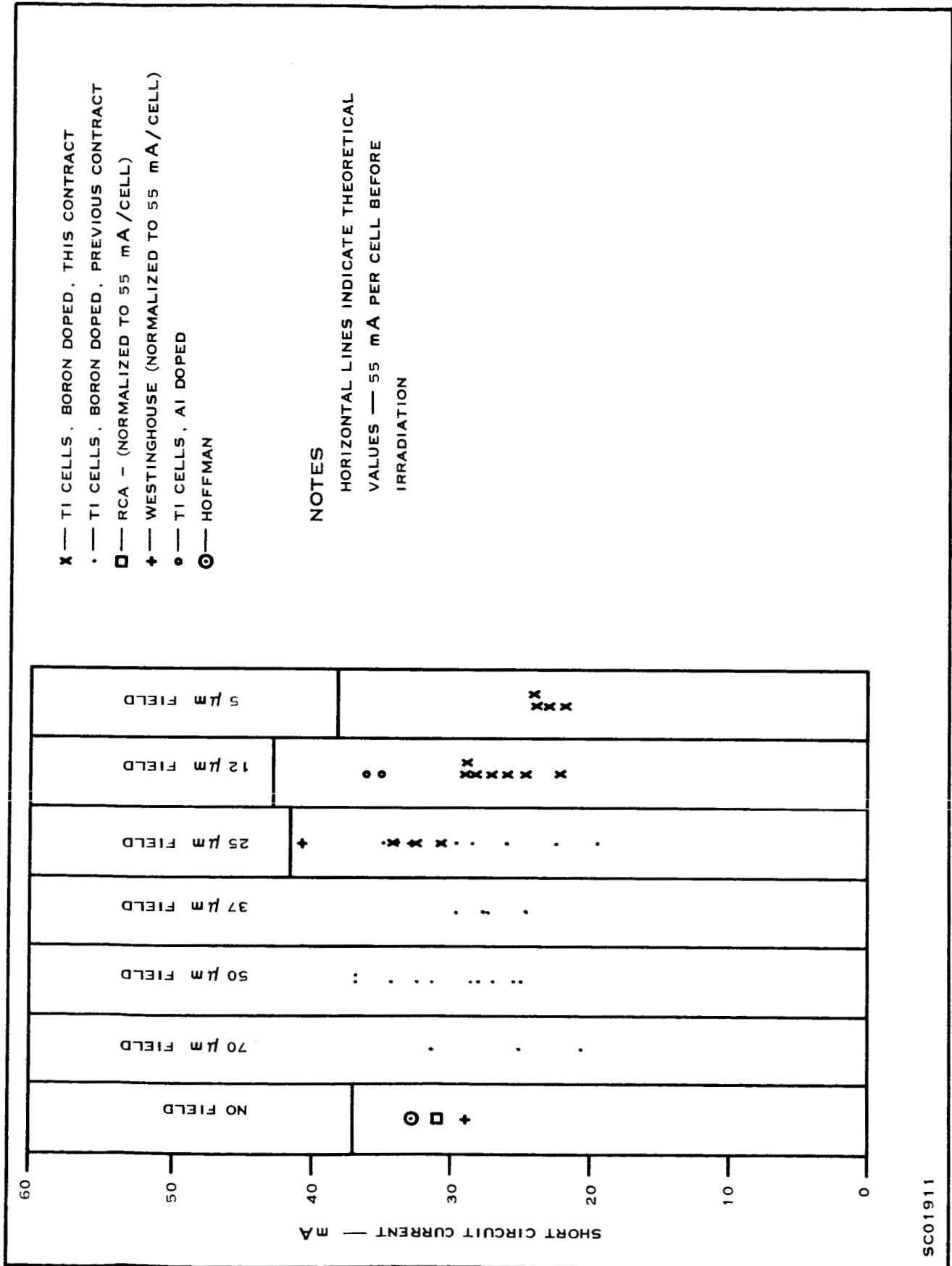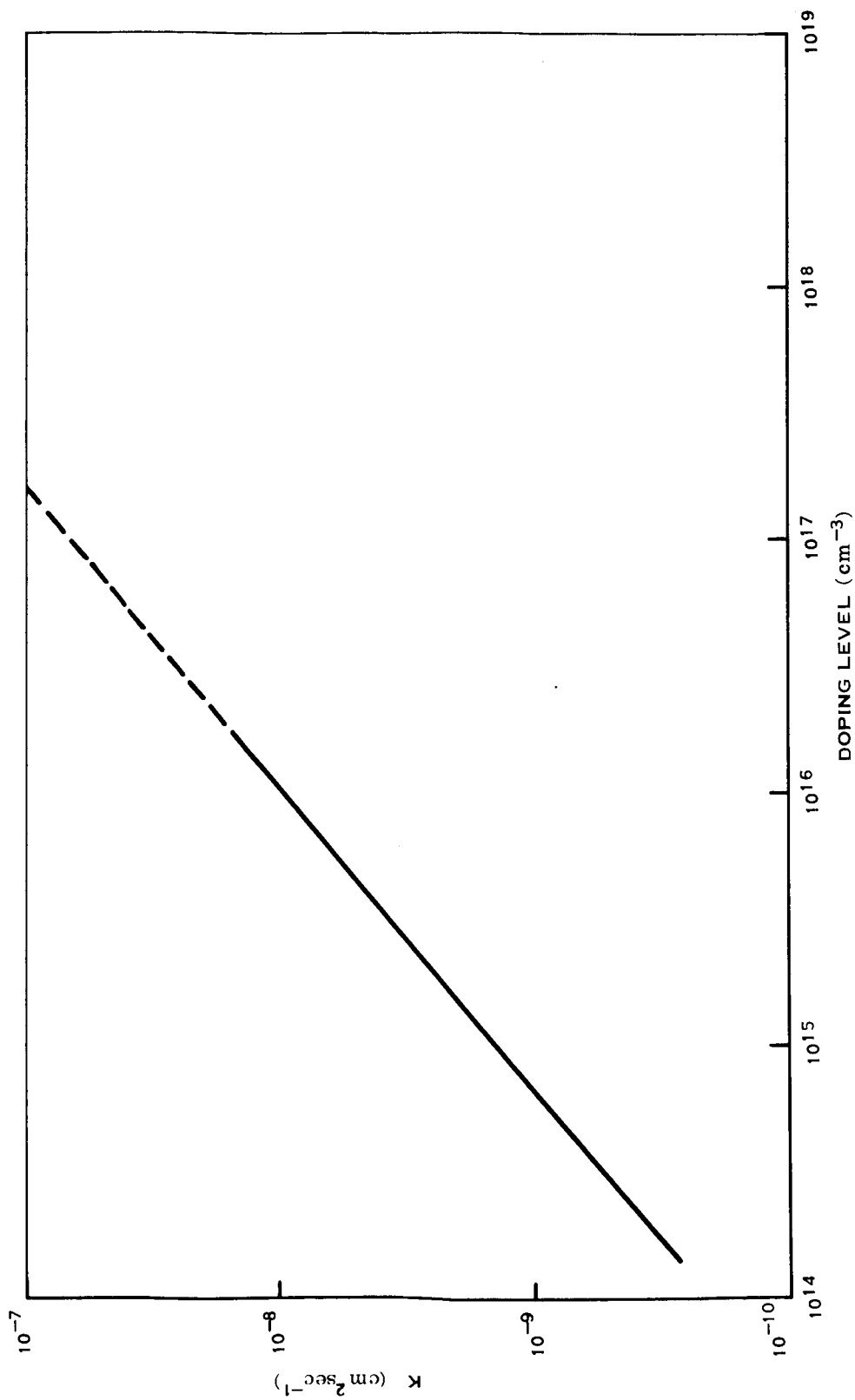
Figure 23. Current Remaining After 10^{16} e/cm^2

SC01911

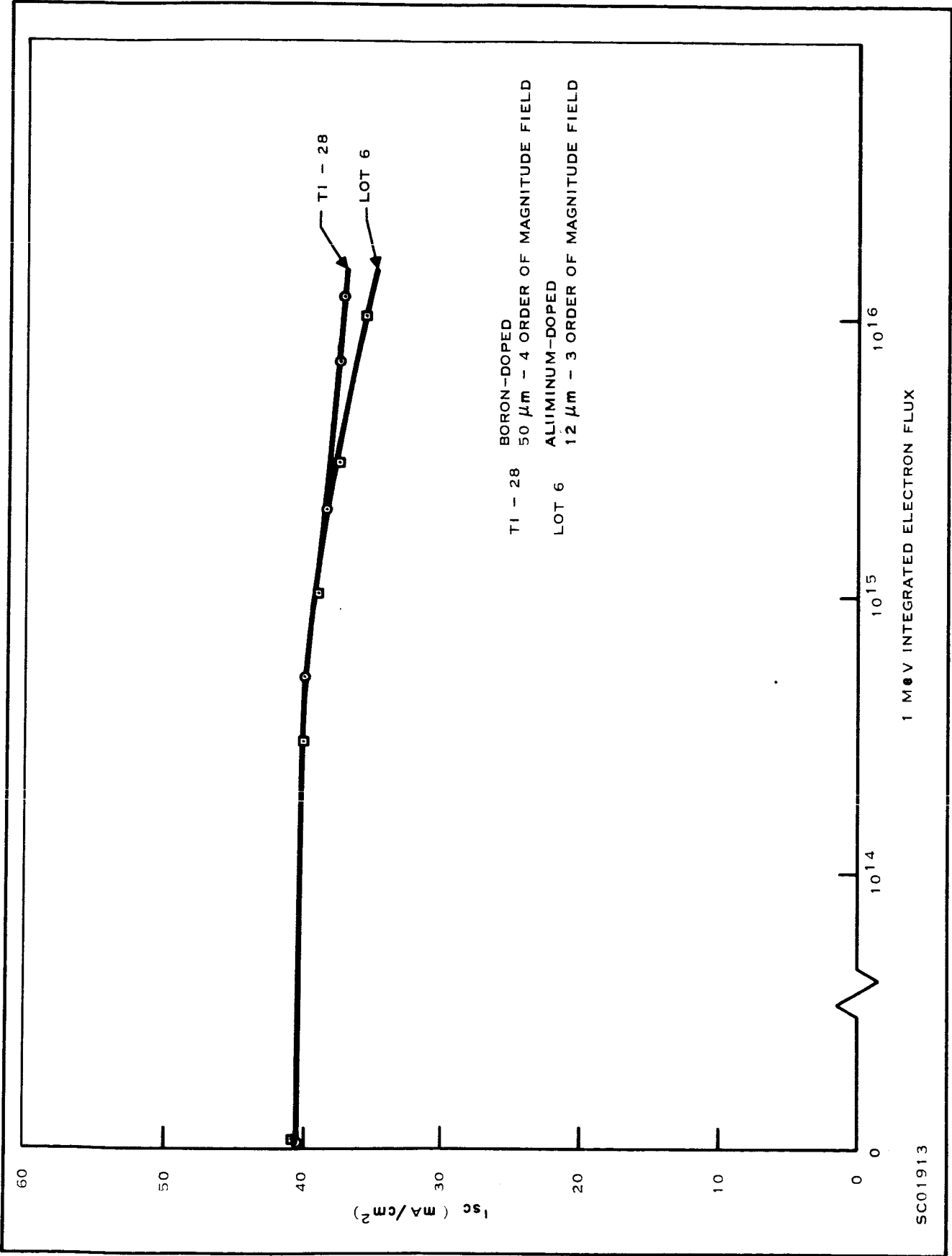Figure 24. K versus Doping Level for 1 MeV Electrons

SC01912

Figure 25. Comparison of Two Cells with Low Current Degradation

SC01913

SECTION V

IMPURITY CONCENTRATION PROFILE STUDIES

A. GENERAL

As mentioned in an earlier section, time-temperature diffusion conditions were selected, based on available diffusion coefficient data, to diffuse the substrate impurities into the epitaxial layer such that the diffusion front would reach out to the surface. However, the use of a measurement technique to determine the location of the drift-field and evaluate the diffusion coefficients used in the calculations was deemed desirable. A novel method for the determination of the impurity concentration profile (present in drift-field structures) was developed in the previous contract (Reference 1) and has since been published [6]. Refinement of the profiling technique and use of the technique for determining profiles of actual solar cells were two goals of the present contract.

In order to meet sample cell delivery dates, silicon material was procured prior to the awarding of the contract. The silicon substrates were chemically etch-polished to provide the best surface for the epitaxial deposition. Later experiments revealed, however, that concentration profiles measured on chemically polished material were unsatisfactory due to deviations from planarity present in the chemically polished

---

[6] Stacy B. Watelski, W. R. Runyan, and R. C. Wackwitz, "A Concentration Gradient Profiling Method," J. Electrochem. Soc. 112, 1051-53 (1965).

substrates. Thus, late in the contract period, some mechanically polished, plane-parellel silicon epitaxial material was obtained to use in refining the profiling technique. Results of the impurity concentration measurements on this mechanically polished material afforded an indirect determination of the profiles in the sample cells (except for Lot 6, which was aluminum-doped material).

B.   SAMPLE PREPARATION

A silicon crystal, boron-doped to 0.06 Ω-cm was sawed, lapped and mechanically polished to usual substrate dimensions. Epitaxial layers were grown to a thickness of 25 μm and a resistivity of 10 Ω-cm (p-type). The epitaxial material was divided into five groups and given the diffusions shown in Table III.

Table III.   Material Diffusion Conditions for Profile Studies

Group Number	Diffusion Conditions	
	Hours*	Temp. °C
A	168.1	1200
B	72.1	1200
C	18.3	1200
D	4.8	1200
E	0.3	1200

* Includes epitaxial cycle time of 0.3 hour at 1200°C

These groups were the starting material for the profile measurements. A minimum of three samples per group were selected for profiling.

The sample preparation prior to angle grinding, the method of obtaining raw data, and the metallographic sectioning were all as given in the previous contract [1].

C. DATA TREATMENT AND RESULTS

The original computer program description described by Watelski et al [6] has been modified such that the raw data are used as the computer input data. The program now consists of two separate programs. The first program results in a tape output (which is used as the second program input) and two computer-plotted curves relating 1) depth versus length (Figure 26), and 2) sheet resistance versus depth (Figure 27). Figure 26 is actually a smoothed plot of the surface of the bevel-ground sample over its entire length and represents that path actually taken by the four-point probe (Figure 28). The zero value on the ordinate of Figure 26 corresponds to the four-point probe reading made at the reference index. Positive and negative values correspond to the respectively marked polarity positions of Figure 28. The abscissa is the thickness of the sample. The square symbols represent measured values. The sheet-resistance versus depth curve contains actual raw data points. Figures 26 and 27 are optional and are used for reference only.

The second program is the critical one. It smooths the sheet-resistance-versus-depth curve, calculates resistivity and presents three graphs, in addition to a printed numerical output. These graphs are:

1) Sheet conductance versus depth

2) Log of the absolute magnitude of the first derivative versus depth

3) Impurity concentration versus depth.

Representative graphs of sheet conductance and concentration are given for each of the five diffusion groups (Figures 29 through 38), and a first-derivative curve is included from group A (Figure 39). The sample number given on each graph contains a letter which identifies the sample group. Unfortunately, groups C and D, which had the

shortest post-epitaxy diffusion times, contained both p- and n-type areas within their layers. Group E, which had no post-epitaxy diffusion, also contained p- and n-type regions. In spite of these junction areas, the data presented on the graphs are correct through the substrate and the epitaxial layer to the junction region. The computer program is not capable of following a p-n junction.

Many factors affect the quality and accuracy of the concentration-versus-depth curves. Such factors are:

1) Polynomial-power coefficient probability

2) Smoothing power

3) Number-of-points smoothed

4) Number of repeat-smoothing cycles.

Local smoothing is used to smooth the log-sheet-conductance-versus-depth curve. The power of the orthogonal-polynomial power series to be fitted to each n-points within the curve, progressing along it by using n-point smoothing, is determined such that one fits the highest power series possible (not to exceed seven). The regression coefficient of the highest power term in the series must be significantly non-zero at the selected polynomial-power coefficient probability[7] (usually 5 percent). That is, the regression coefficients of the highest power term of the next two higher power series would be considered zero at that probability level. Hence, a power is so obtained for each n-points smoothed, progressing along the curve. When the curve-smoothing is completed, the powers so obtained are averaged, rounded off to the nearest integer power and used for repeat-cycle curve smoothing.

7/   A. Hald, "Statistical Theory with Engineering Applications," John Wiley & Sons, New York (1960), pp 638-42.

The program subroutine can be automatic such that it will fit the proper powers to the array, or it may be pre-set to any power. This smoothing power should be ≥ 2. If a smoothing power of 2 is indicated, then the resulting curve is critically judged for logical correctness, i.e., does it seem like the results obtained are feasible? The automatic smoothing routine will begin with a seven-point local smooth, then it will repeat the seven-point smooth on the already smoothed curve. A figure of merit [8] (sum of the squares of the third derivative) is then calculated. The local smoothing is advanced to nine points with another two-cycle repeat and another figure of merit is calculated. This process is continued until a minimum figure of merit is obtained, followed by at least four consecutive figures of merit which are greater in magnitude. The local point smoothing corresponding to the minimum figure-of-merit value is accepted and tried with increasing numbers of repeat cycles to arrive at another minimum figure of merit. A typical set of values is shown in Table IV. The minimum value of the figure of merit is shown for a variable number of smoothed points (starting at 21) along with the associated four larger figures of merit (numbered in parentheses). Then the number of repeat cycles associated with a minimum figure of merit is shown. Although the number of repeat cycles is one, the program is set to accept a minimum of two; hence, the data presented in the last line will be used for this particular sample.

An example of the way in which the number of smoothing points can affect a curve is shown in Figures 40, 41, and 30 for sample No. A-16. Table V shows descriptive data for the smoothing points.

---

[8] F. Theilheimer and W. Starkweather, "The Fairing of Ship Lines on a High-Speed Computer," Math. Comp. 15, 338-55 (1961).

Table IV. Typical Set of Smoothing Data

Smoothed	No. Cycles Repeat	No. Points Rejected	Figure of Merit	
			Value	Magnitude
21	2	5	1.834×10^{15}	
23	2	3	1.802×10^{15}	Min
25	2	4	1.814×10^{15}	(1)
27	2	7	1.822×10^{15}	(2)
29	2	4	1.810×10^{15}	(3)
31	2	6	1.861×10^{15}	(4)
23	1	3	1.790×10^{15}	Min
23	2	3	1.802×10^{15}	
23	3	3	1.802×10^{15}	
23	4	3	1.801×10^{15}	
23	5	3	1.800×10^{15}	
23	2	3	1.802×10^{15}	

Table V. Smoothing-point Data for Curves in Figures 40, 41 and 30.

Figure No.	Smoothing Points	Repeat Cycles	Smoothing Power
40	7	2	2.000
41	23	2	3.000
30	31	10	4.000

Note that the sheet conductance of all three curves (Figures 42, 43, and 29) look very much alike. Figure 42 with its seven-point smoothing reacts to the kink in the curve (at~7 μm). A larger number of smoothing points (Figures 43 and 29) does not see this kink. This anomalous kink, as well as smaller ones, can be eliminated by the judicious choice of these smoothing factors.

Additional features could be added to the program to make it more automatic. However, in its current state, the program, supplemented by wise operator judgements, can be very useful in performing its assigned task. The complete program was developed and funded by Texas Instruments; the government contract supplied funding for the calculation and plotting of real problems only.

An idea of the reproducibility of the technique is given by examination of the results of four samples from group B. Group B was essentially identical in character to the material in Lot 3 of Table I. Tabulated in Table VI are the distances in micro-

Table VI. Impurity Concentration Profiles for Group B

Sample Number	Concentration, Atoms cm^{-3}			
	5×10^{17}	1×10^{17}	1×10^{16}	1×10^{15}
	Distance in μm			
2-2	24.8	14.4	7.4	2.9
2-8	27.0	18.5	*	*
2-13	25.5	14.4	7.4	0.8
2-15	28.2	15.2	10.2	2.7

* Sample broke during sectioning

meters at which the impurity concentrations are respectively 5×10^{17}, 1×10^{17}, 1×10^{16}, and 1×10^{15} boron atoms/cm^3 of silicon. The average distance at which the 5×10^{17} value occurs is 26.4 μm. The epitaxial interface, at which that concentration is expected, $N_2/2 = 5 \times 10^{17}$, is 25 μm. These data give an idea of the precision and accuracy of the technique.

Diffusion conditions for group B were designed to diffuse the impurity front out almost to the surface. Extrapolation of the profile to the epitaxial layer concentration, $N_1 = 1 \times 10^{15}$, yielded an average distance of 2.1 μm for the diffusion front at that concentration. Since the diffusion coefficients used [9] to calculate conditions were the same both for the sample solar cells and for the profile samples, and since the closeness of approach of the diffusion front to the surface, for group B, is approximately as desired, it is concluded that the drift fields in sample Lots 1 through 5 terminate immediately adjacent the surface. Profiling was not done on aluminum-doped samples such as Lot 6. Diffusion calculations for this lot were made using the coefficients of Fuller and Ditzenberger [10].

The diffusion coefficient for boron can be computed using the data obtained from sample groups A through E. This coefficient would be unique in that it would have been derived from an all-boron-doped system (i.e. epitaxial layer and substrate).

9/   A. D. Kurtz and R. Yee, "Diffusion of Boron into Silicon," J. Appl. Phys. 31, 303-05 (1960).

10/   C. S. Fuller and J. A. Ditzenberger, "Diffusion of Donor and Acceptor Elements in Silicon," J. Appl. Phys. 27, 544-53 (1956).

DEPTH VS LENGTH

39120908-5 GROUP A   SLICE A
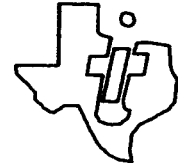
02/15/66
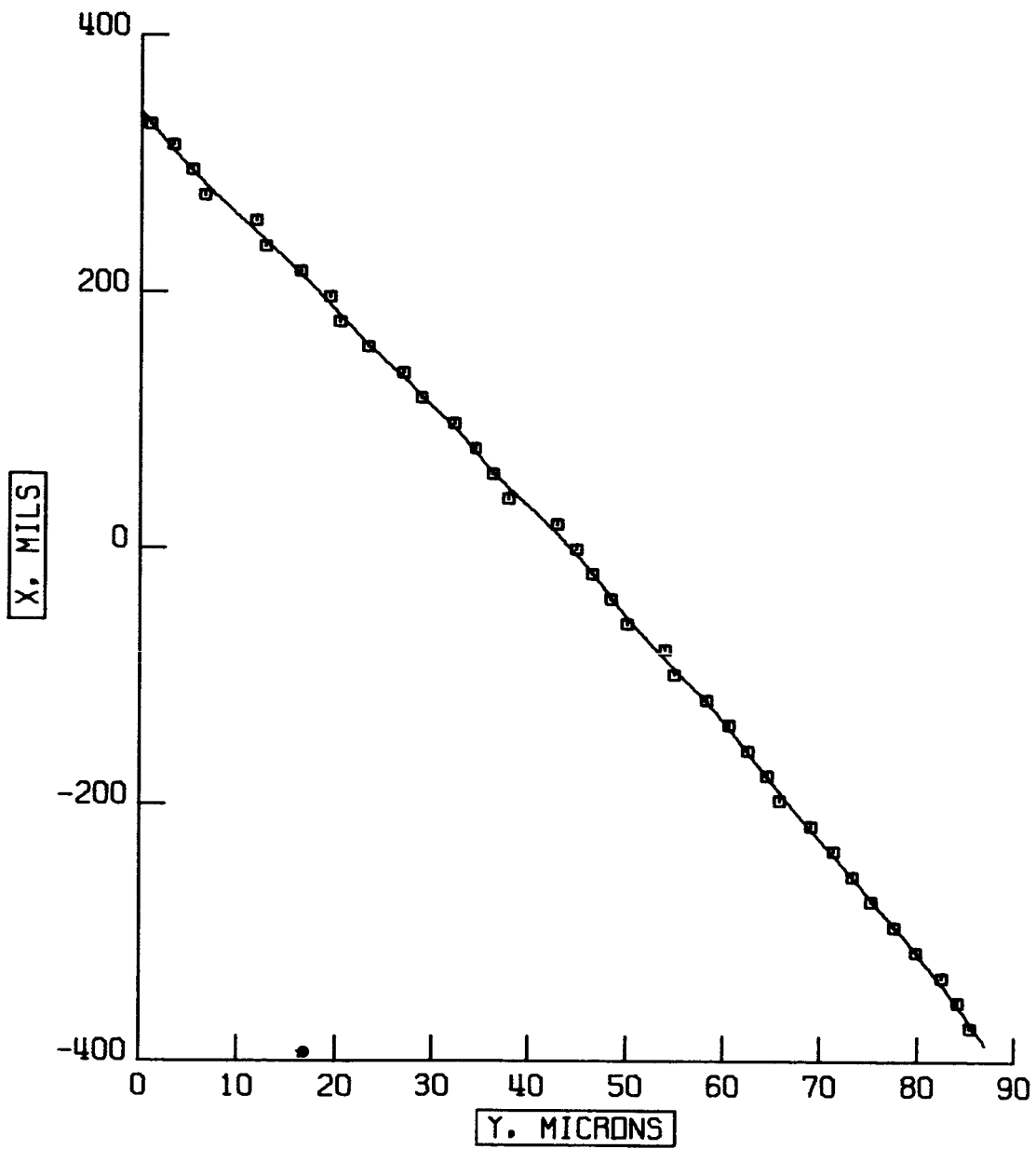
SC01914

Figure 26.   Depth versus Length

SHEET RESISTANCE VS DEPTH

39120908-5 GROUP A   SLICE A
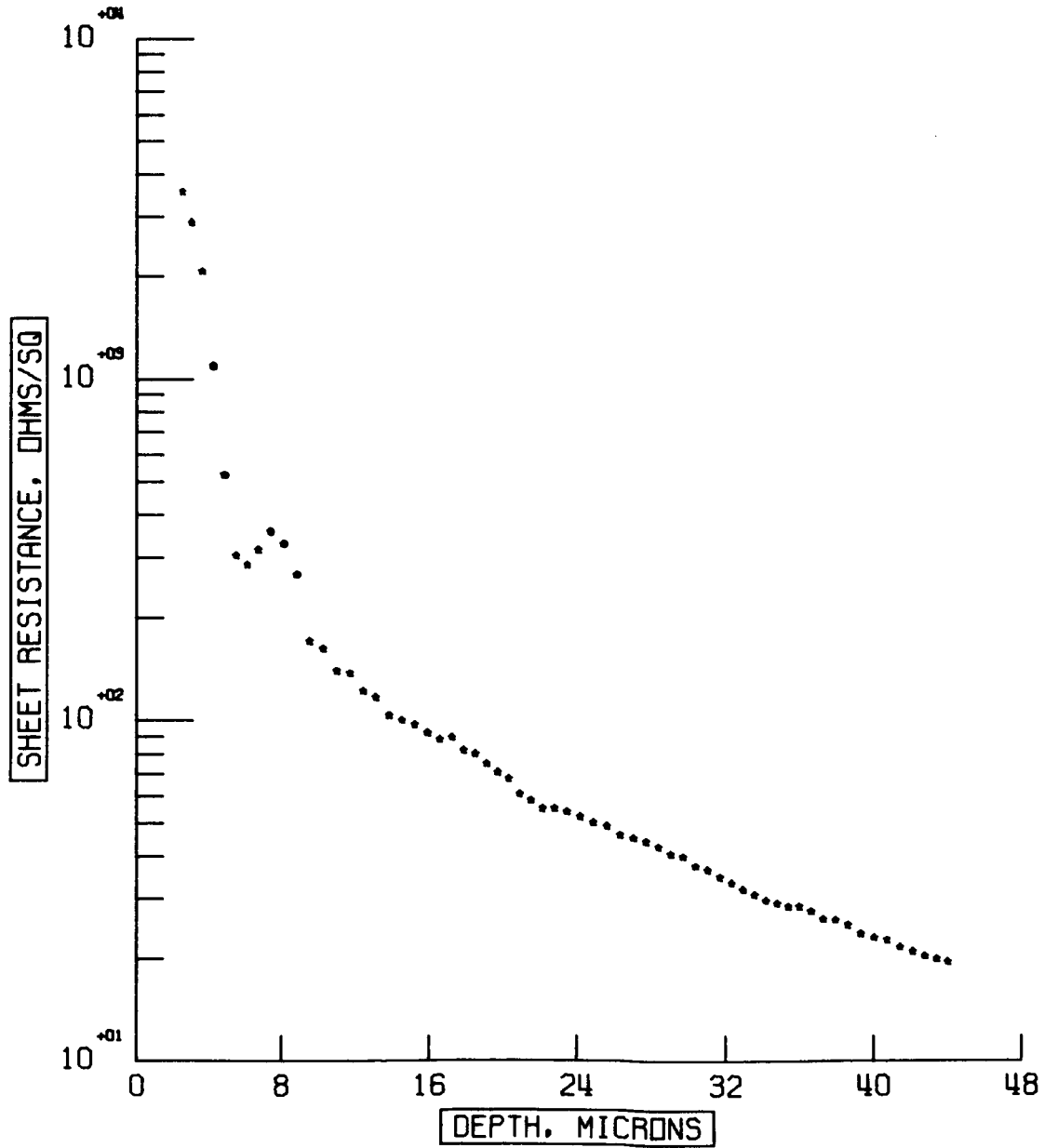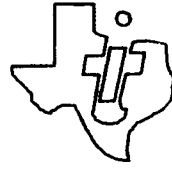
Figure 27.   Sheet Resistance versus Depth
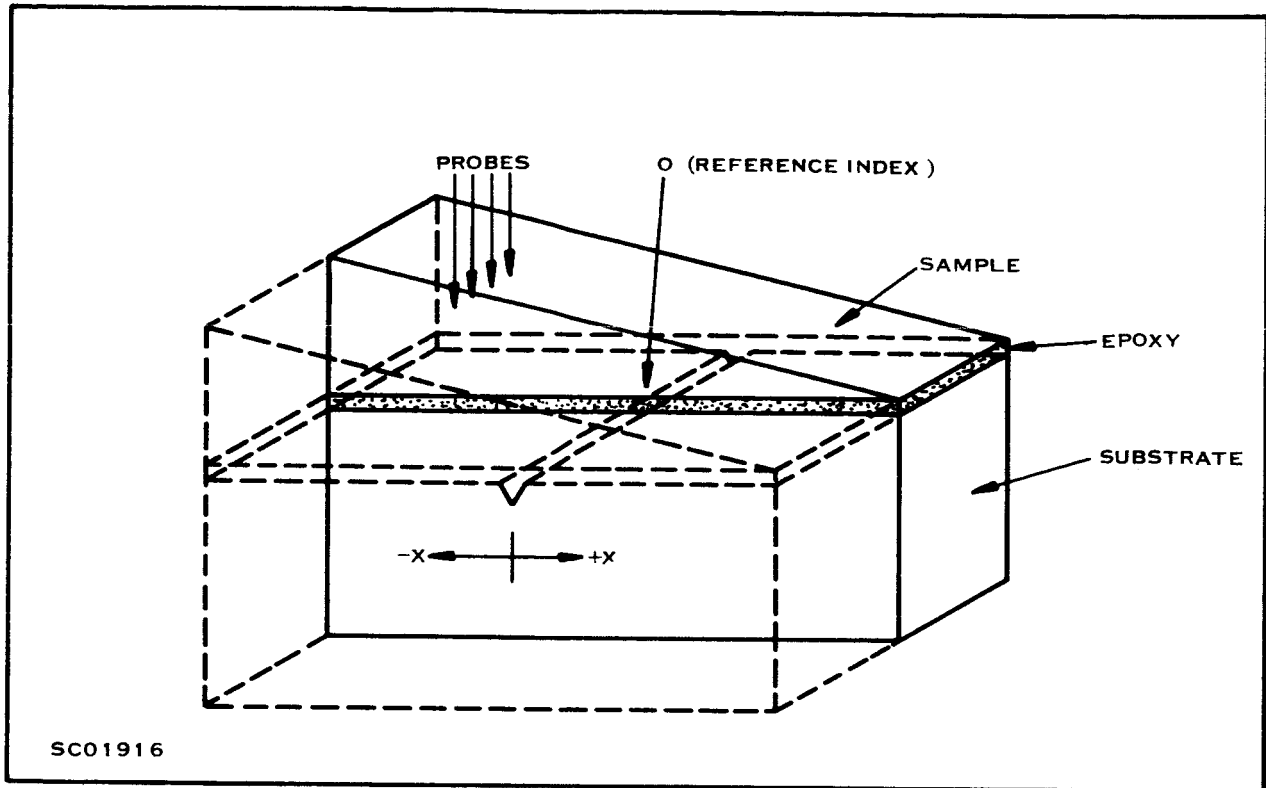
SC01915

Figure 28.   Bevel Ground Sample
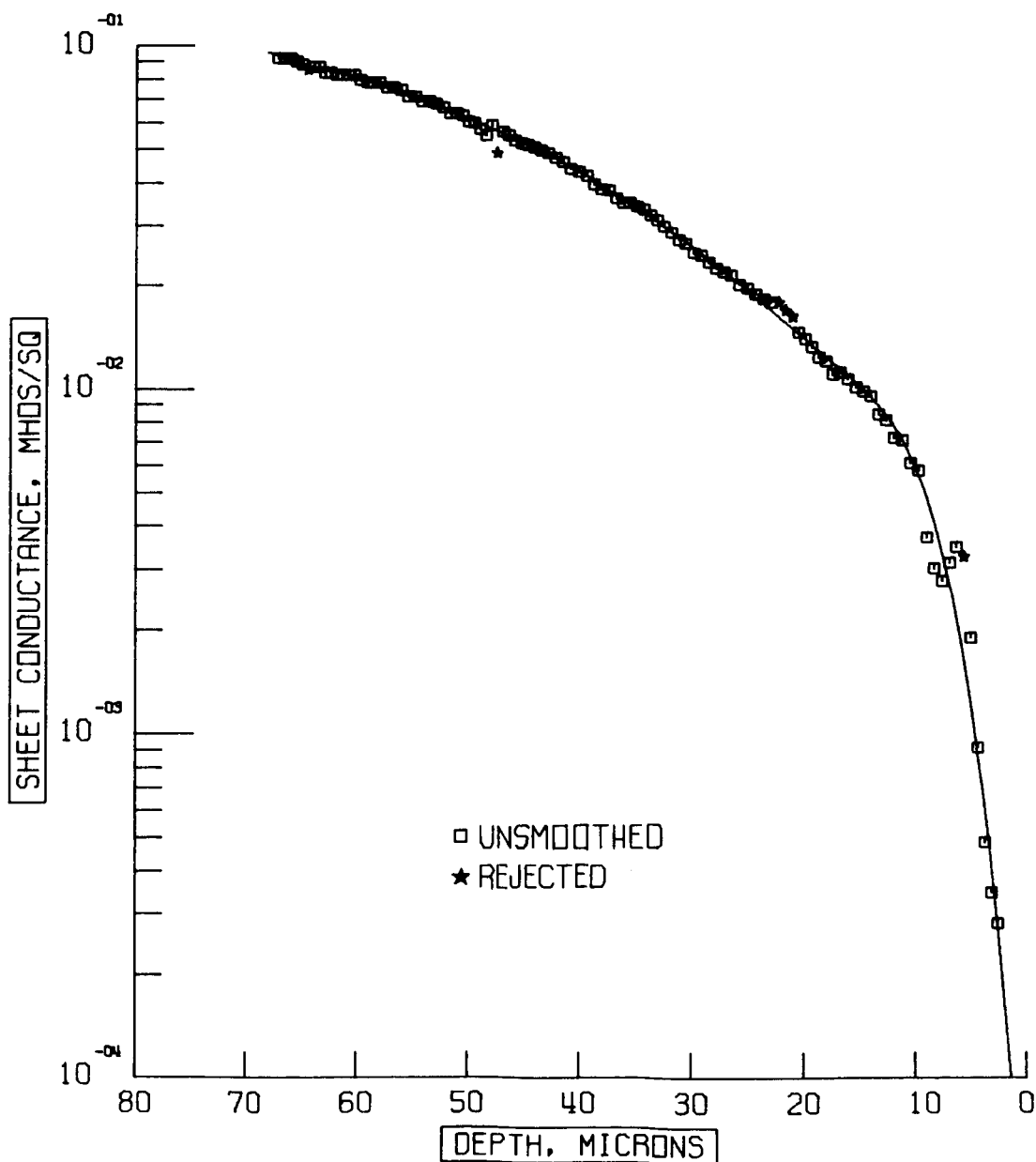
Figure 29. Sheet Conductance versus Depth (Sample No. A-16)
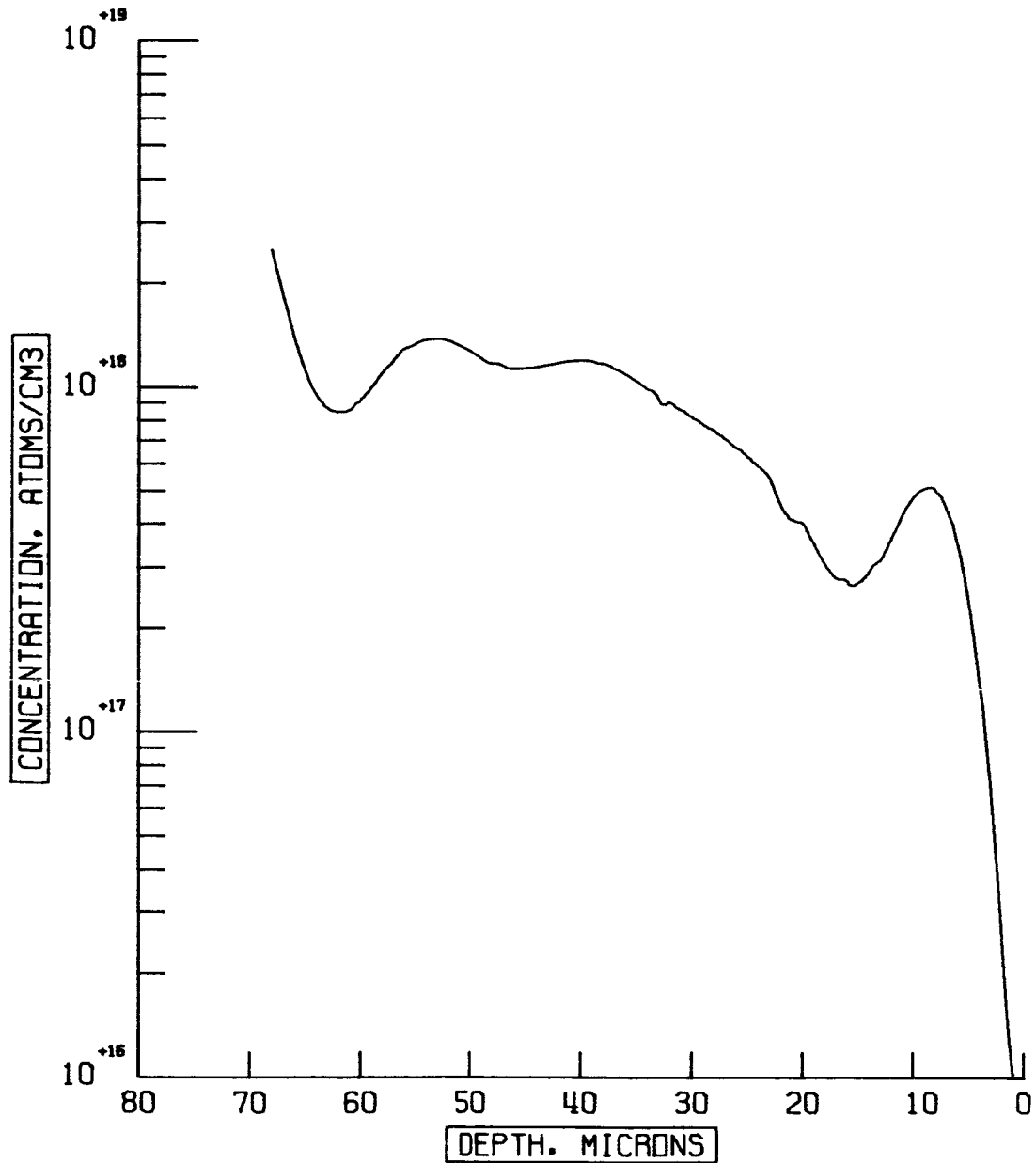
Figure 30.   Concentration versus Depth (Sample No. A-16)

SC01918

Figure 31.   Sheet Conductance versus Depth (Sample No. B-13)

SC01919

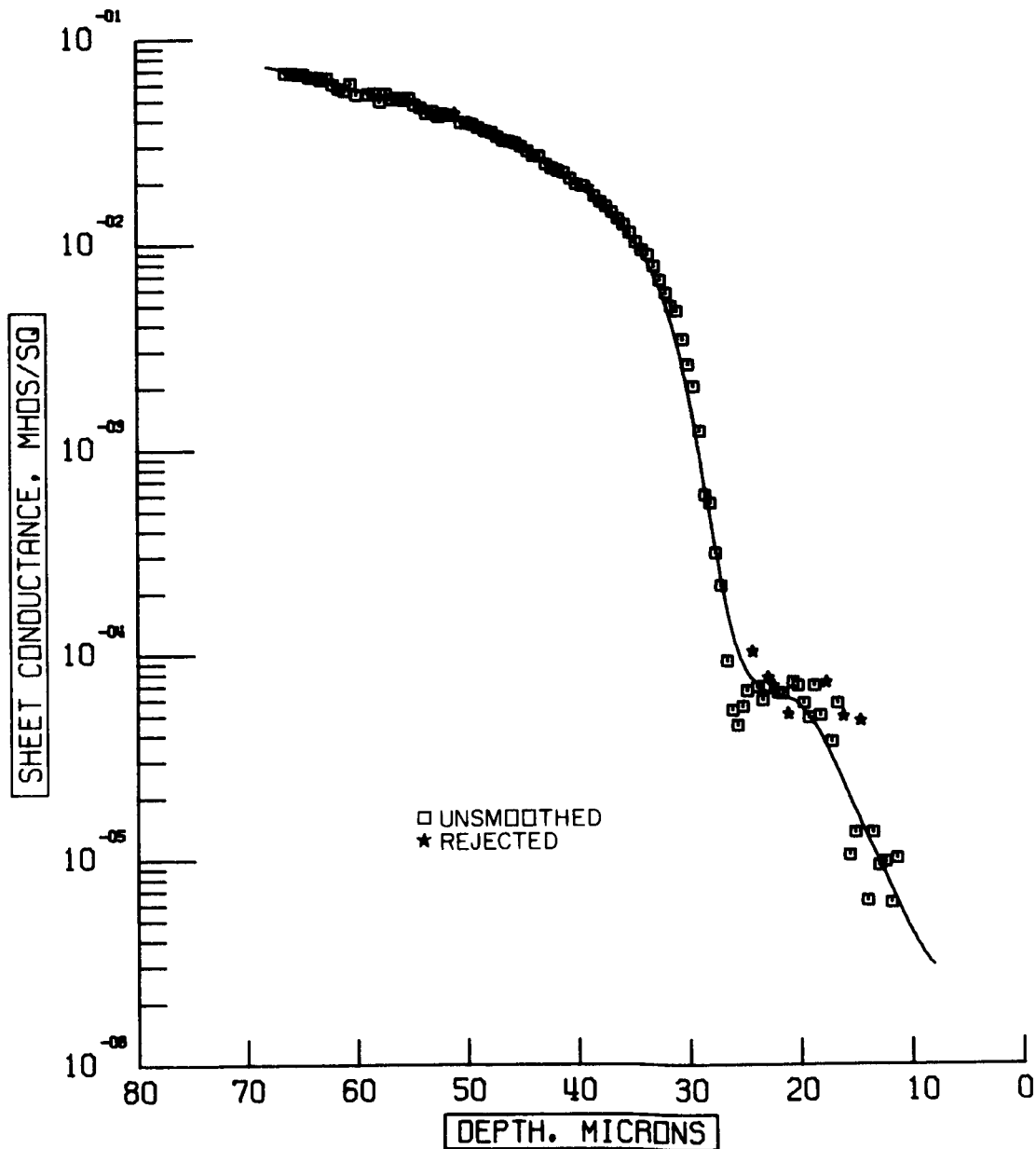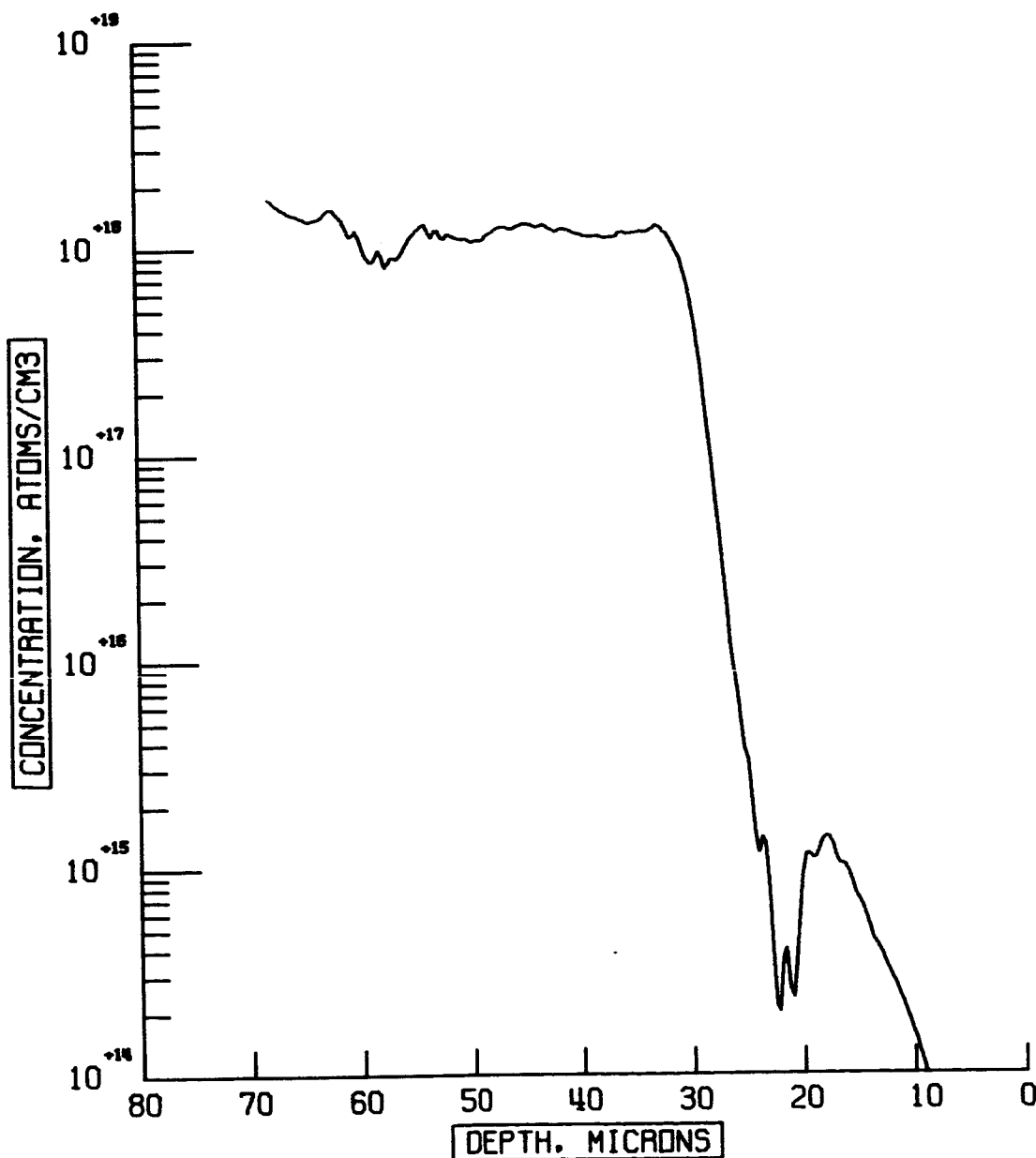DRIFT FIELD SOLAR CELL MATERIAL
(CONTRACT NO. NAS 5-9609)
SAMPLE NO. B-13
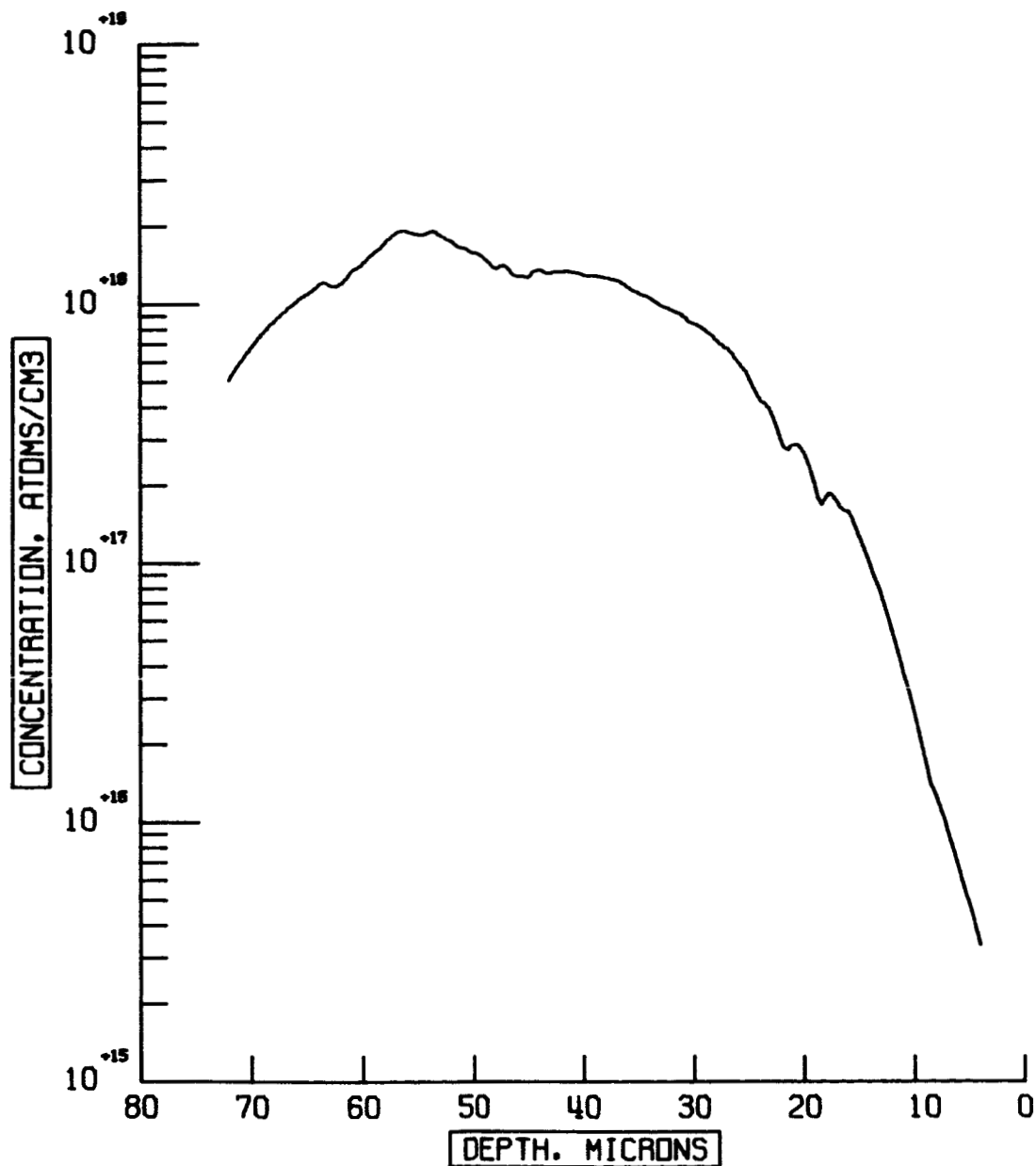
02/17/66

Figure 32.   Concentration versus Depth (Sample No. B-13)

SC01920

DRIFT FIELD SOLAR CELL MATERIAL
(CONTRACT NO. NAS 5-9609)
SAMPLE NO. C-3

02/17/66

□ UNSMOOTHED
★ REJECTED

SHEET CONDUCTANCE, MHOS/SQ

DEPTH, MICRONS
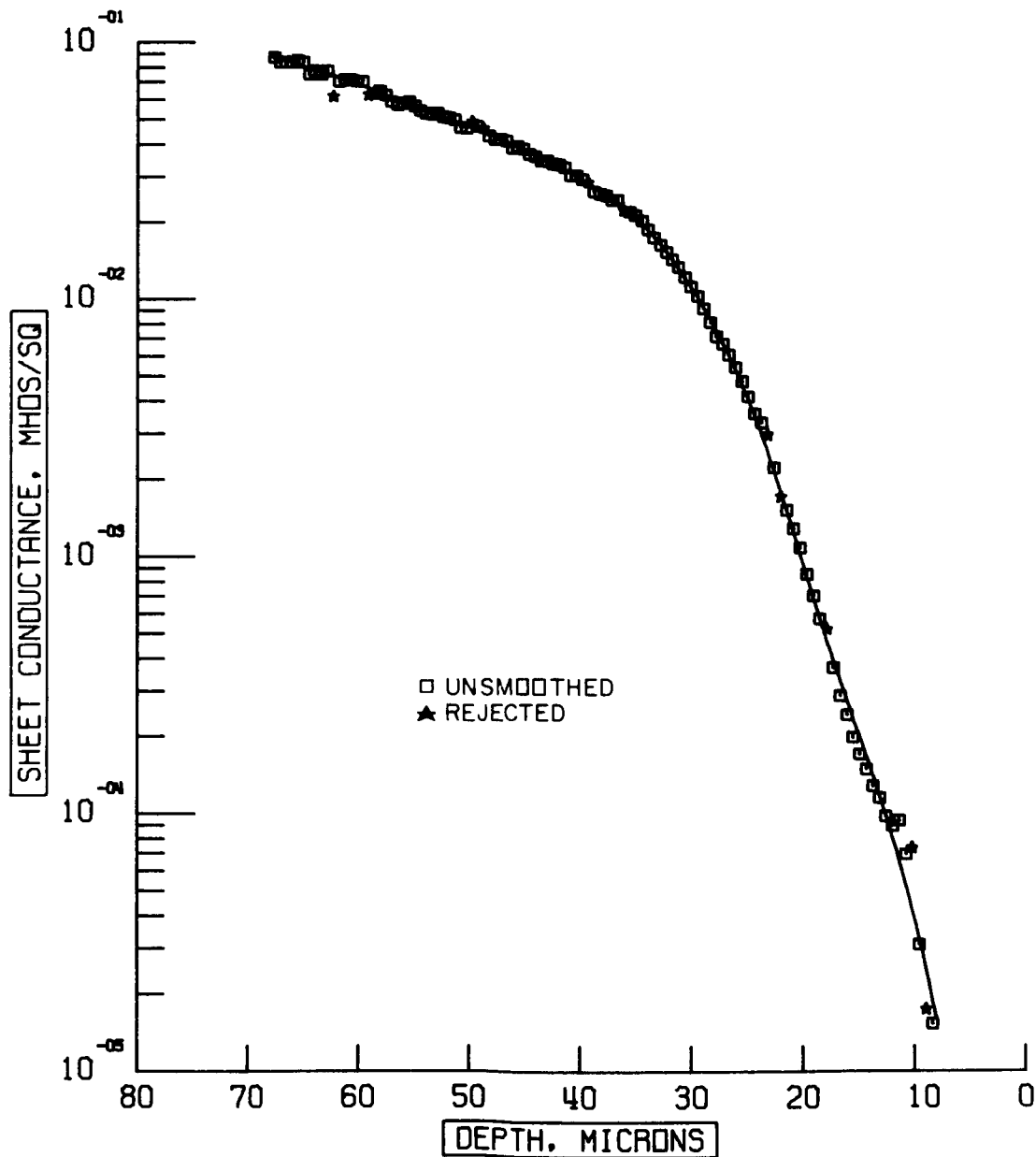
SC01921

Figure 33.   Sheet Conductance versus Depth (Sample No. C-3)
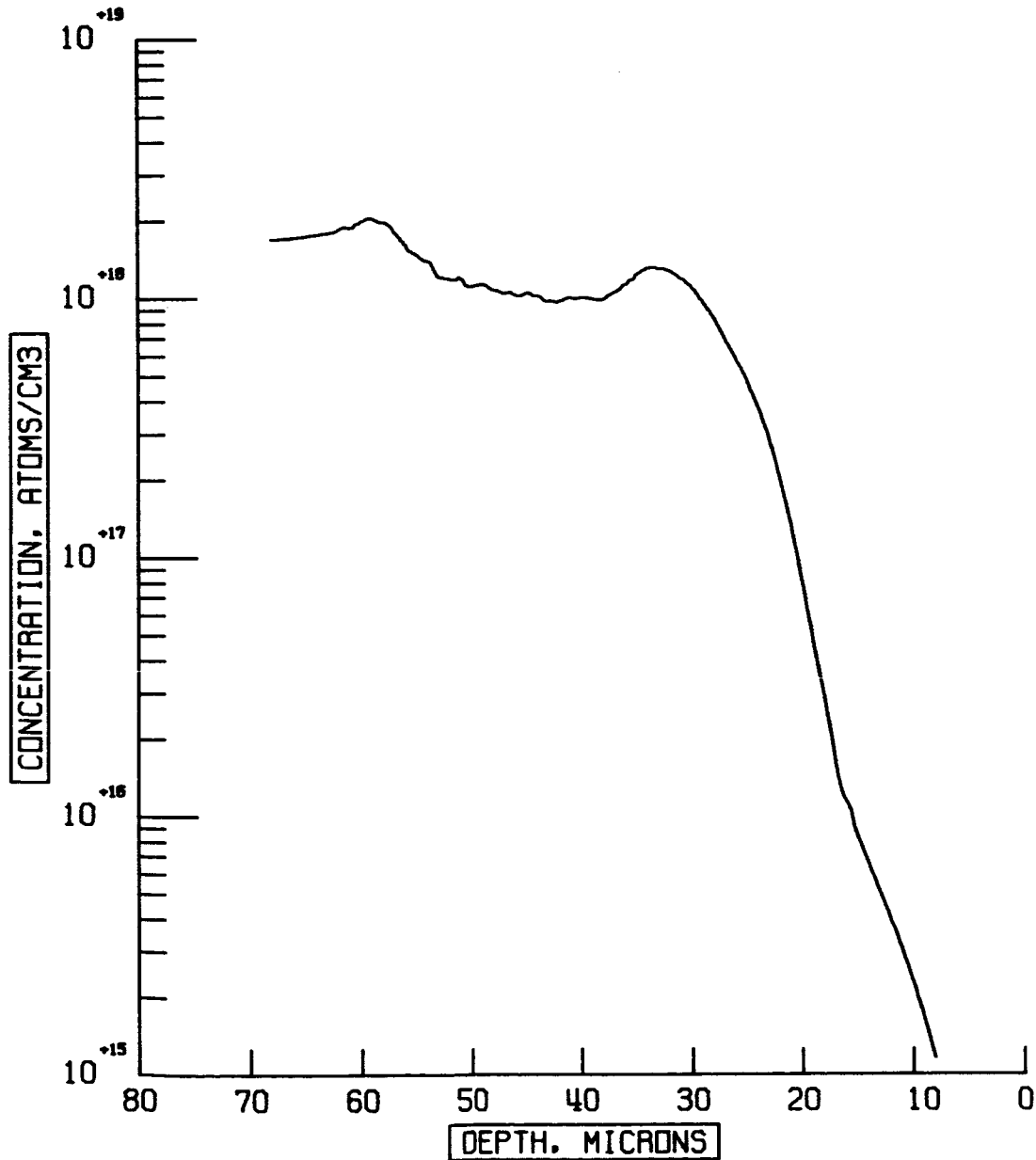
Figure 34.   Concentration versus Depth (Sample No. C-3)
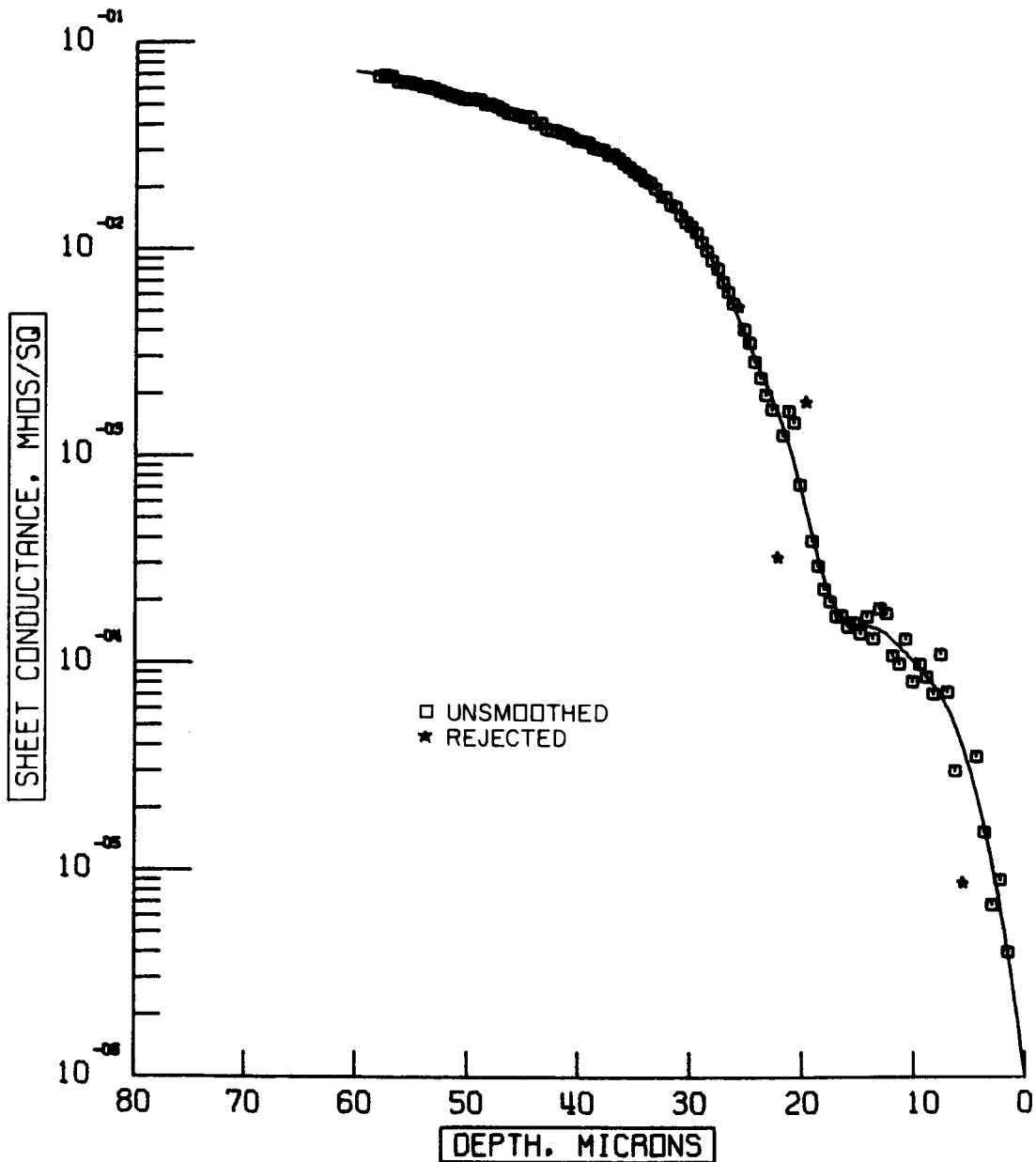
Figure 35. Sheet Conductance versus Depth (Sample No. D-4)

DRIFT FIELD SOLAR CELL MATERIAL
(CONTRACT NO. NAS 5-9609)
SAMPLE NO. D-4
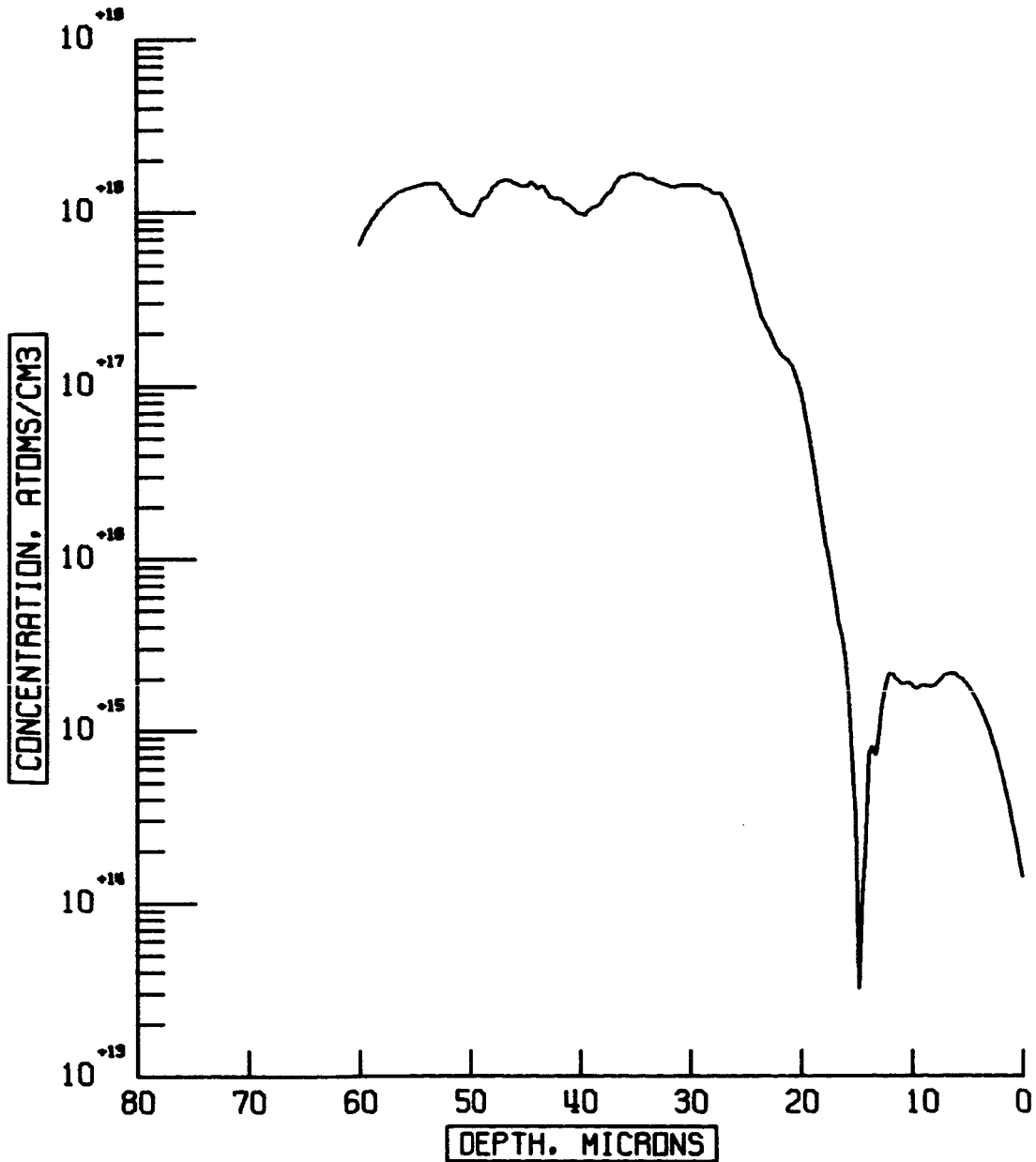
02/17/66

Figure 36. Concentration versus Depth (Sample No. D-4)

SC01924

Figure 37.   Sheet Conductance versus Depth (Sample No. E-5)

SC01925

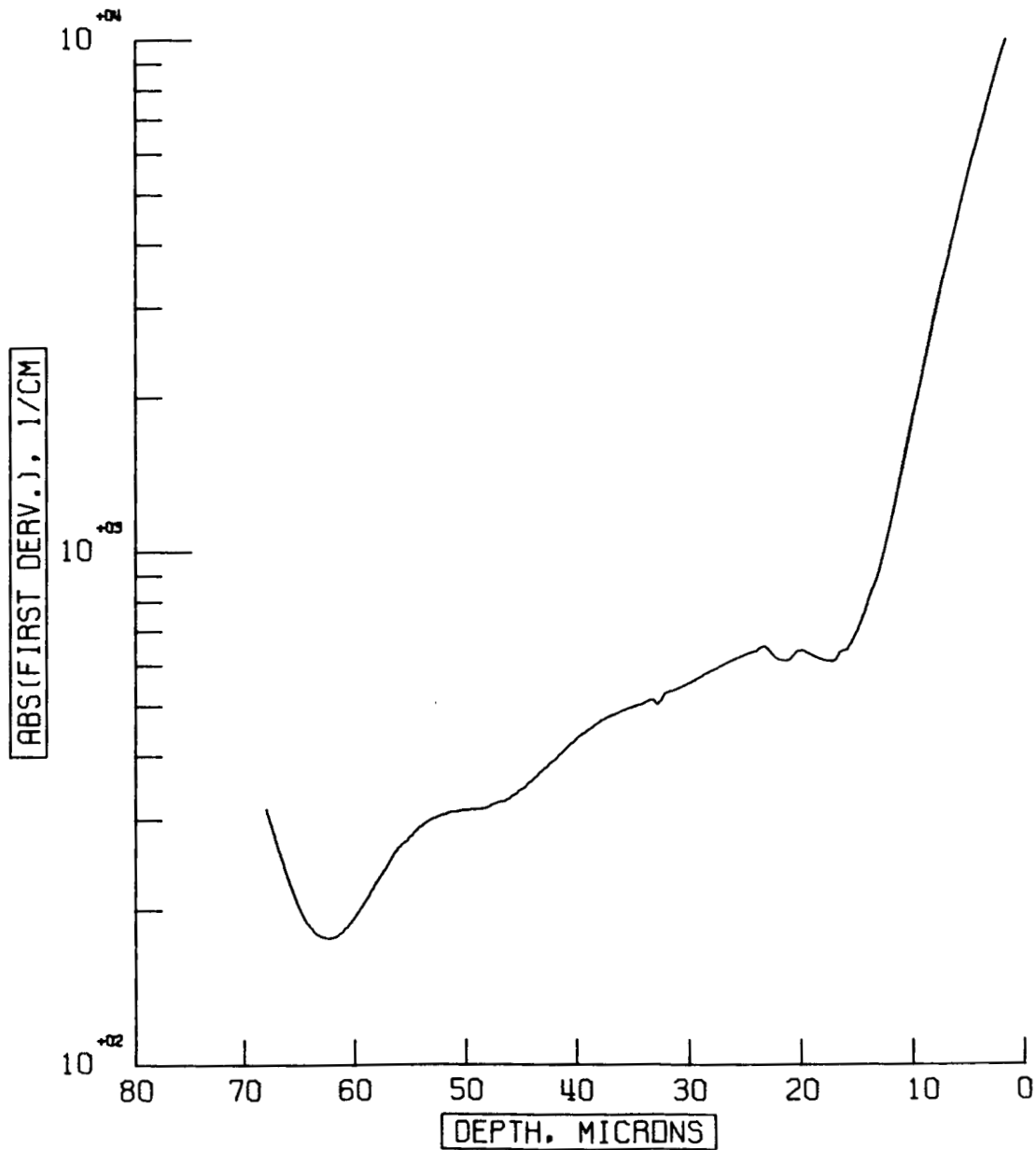DRIFT FIELD SOLAR CELL MATERIAL
(CONTRACT NO. NAS 5-9609)
SAMPLE NO. E-5

02/17/66

SC01926

Figure 38.   Concentration versus Depth (Sample No. E-5)

DRIFT FIELD SOLAR CELL MATERIAL
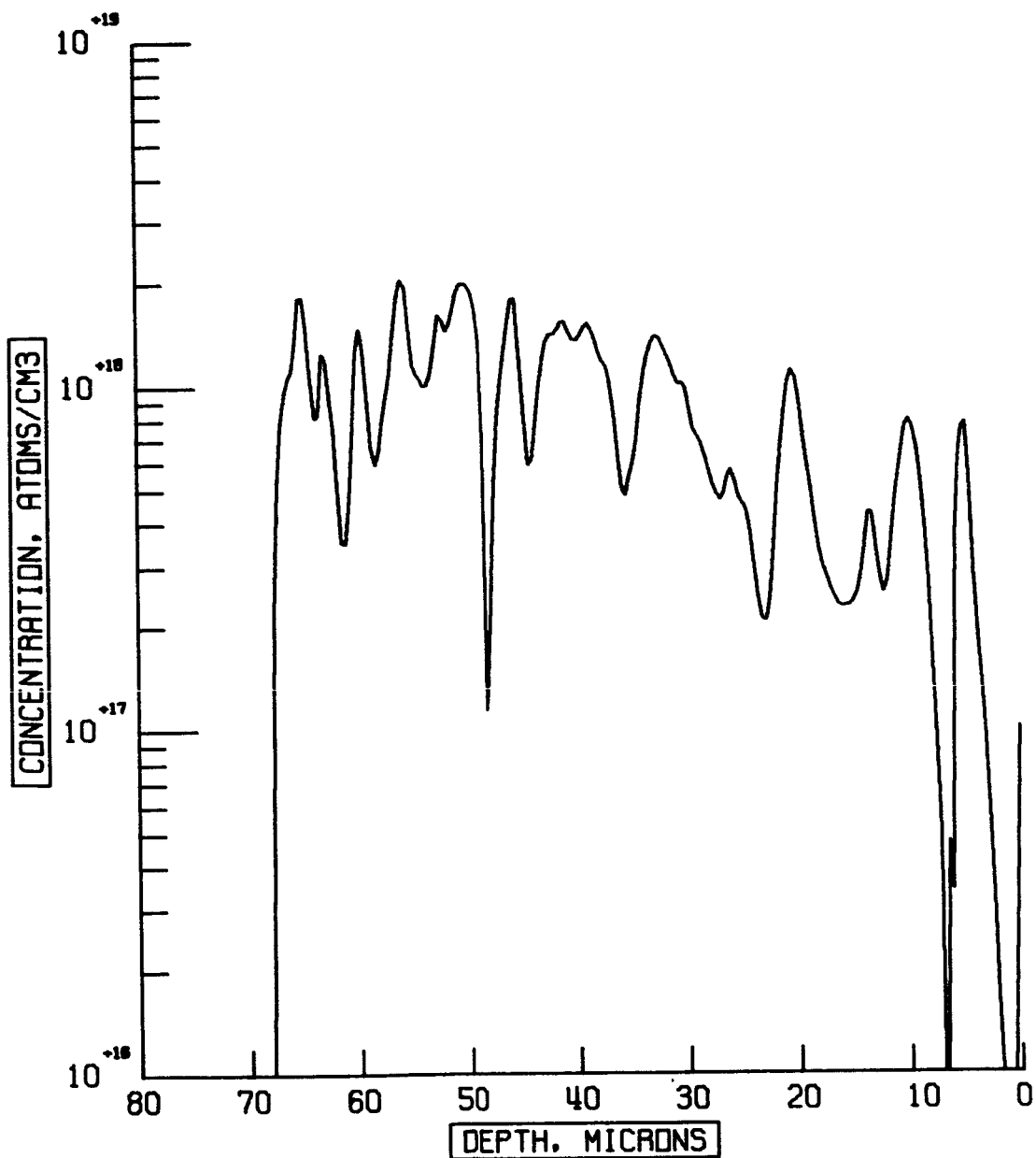(CONTRACT NO. NAS 5-9609)
SAMPLE NO. A-16

02/22/66

SC01927

Figure 39.   Absolute Magnitude of First Derivative versus Depth (Sample No. A-16)

DRIFT FIELD SOLAR CELL MATERIAL
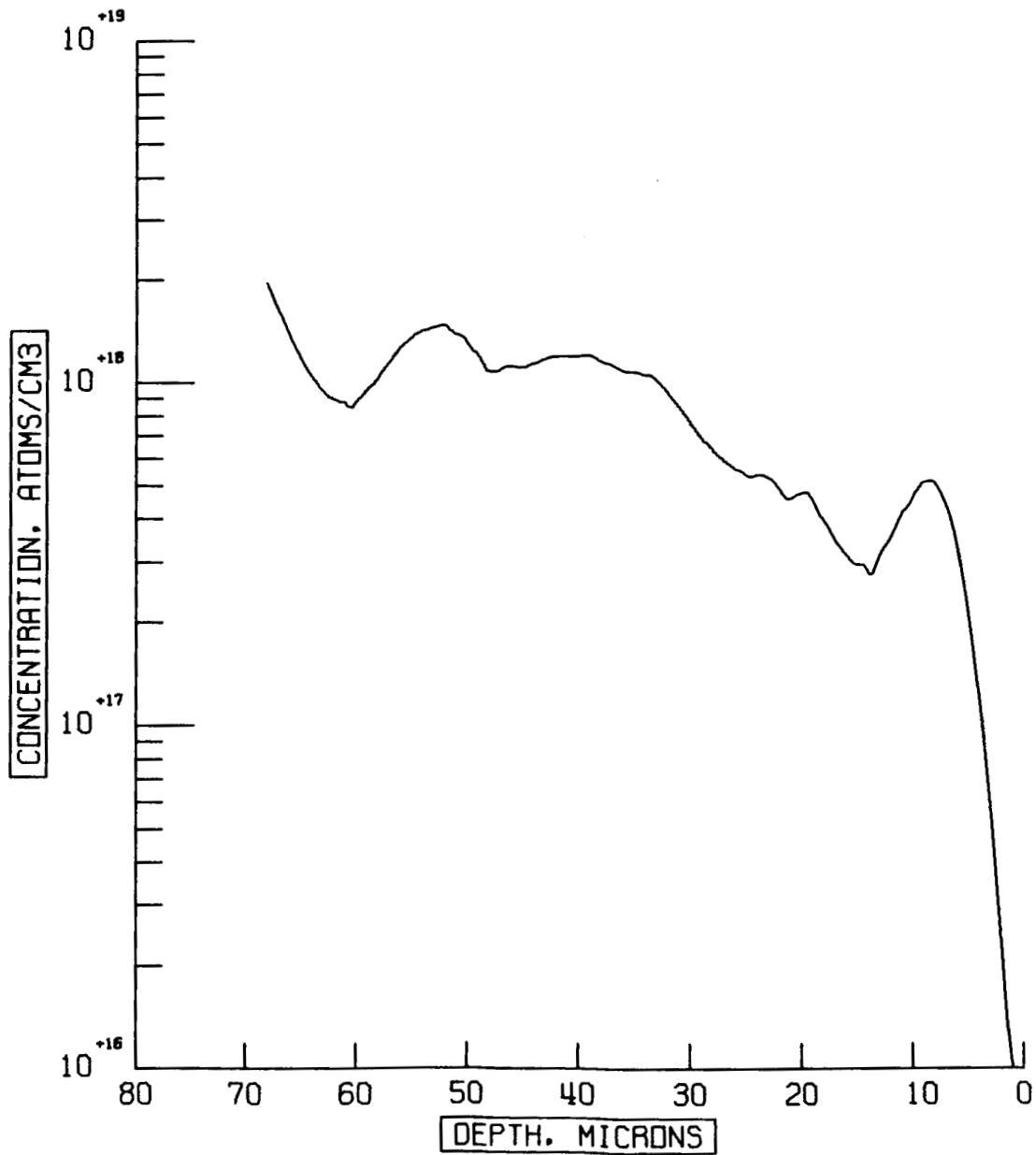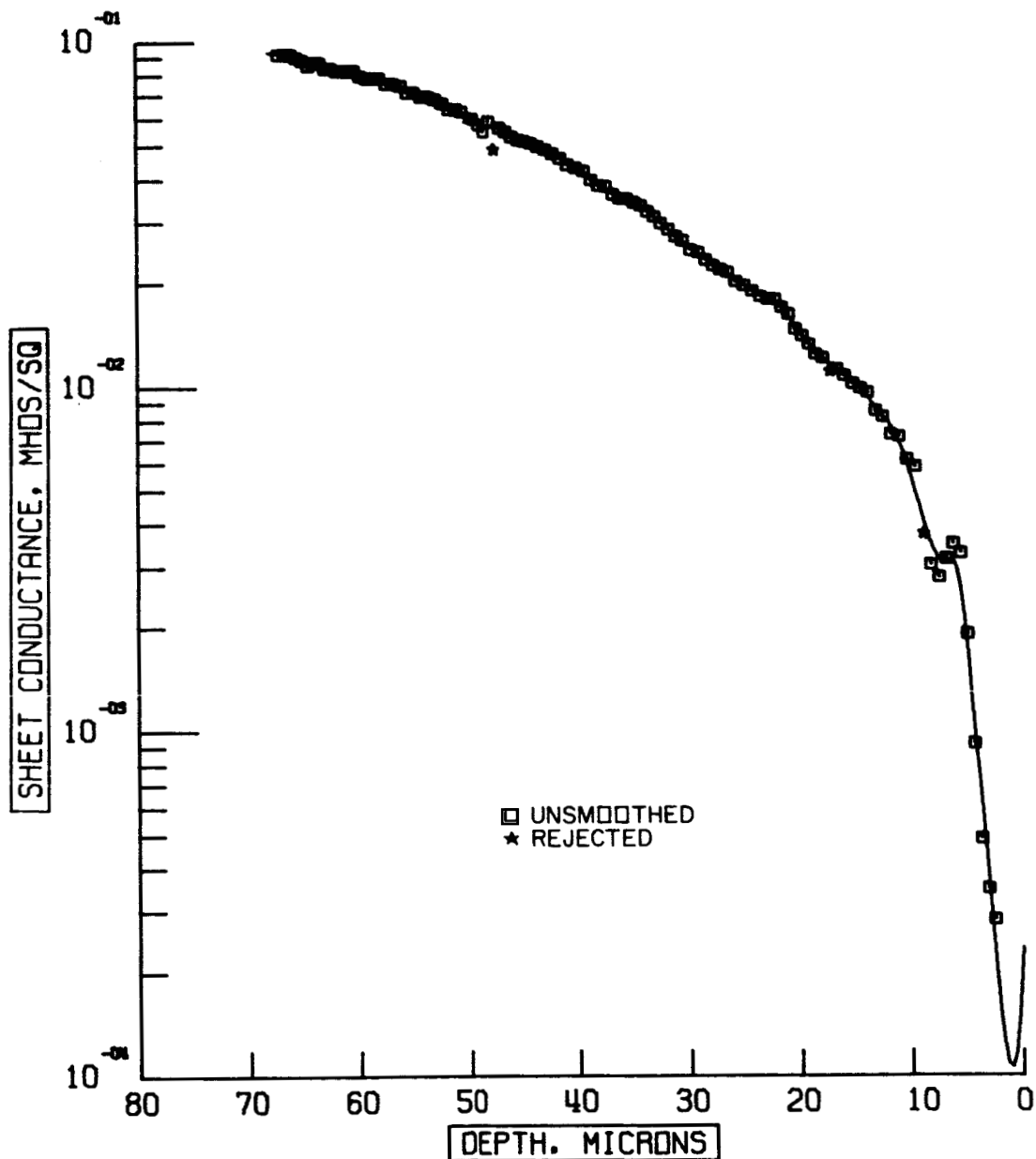(CONTRACT NO. NAS 5-9609)
SAMPLE NO. A-16

02/17/66

SC01928

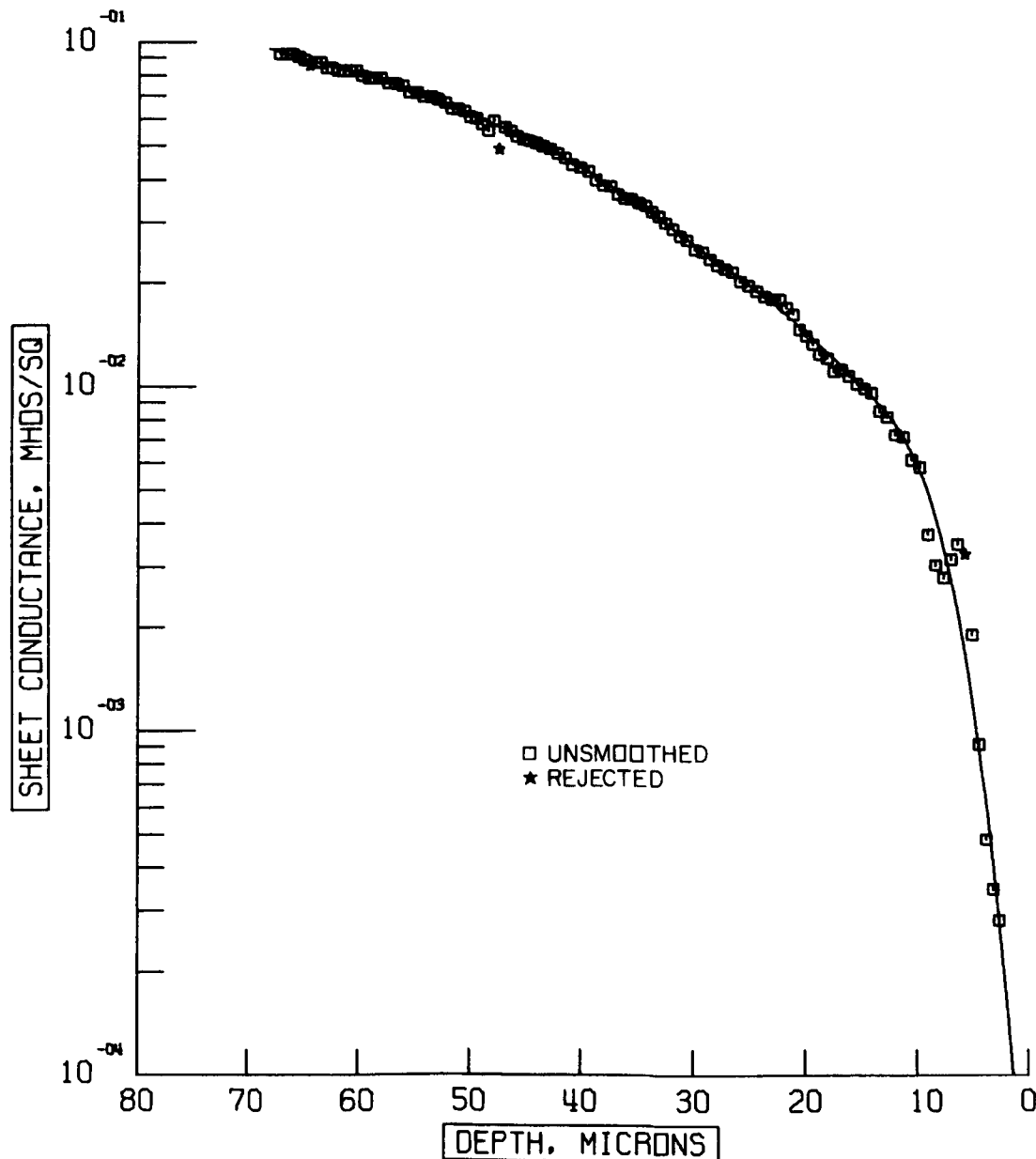Figure 40. Concentration versus Depth (Sample No. A-16)

Figure 41.   Concentration versus Depth (Sample No. A-16)

Figure 42.   Sheet Conductance versus Depth (Sample No. A-16)

Figure 43.   Sheet Conductance versus Depth (Sample No. A-16)

SECTION VI

CELL FABRICATION

All cells for this contract were fabricated using Procedure II as outlined in the final report of Contract NAS5-3559. The flow diagram in Figure 44 shows the process steps that were followed in making the cells.

A photograph of the epitaxial slice after diffusion is shown in Figure 45.
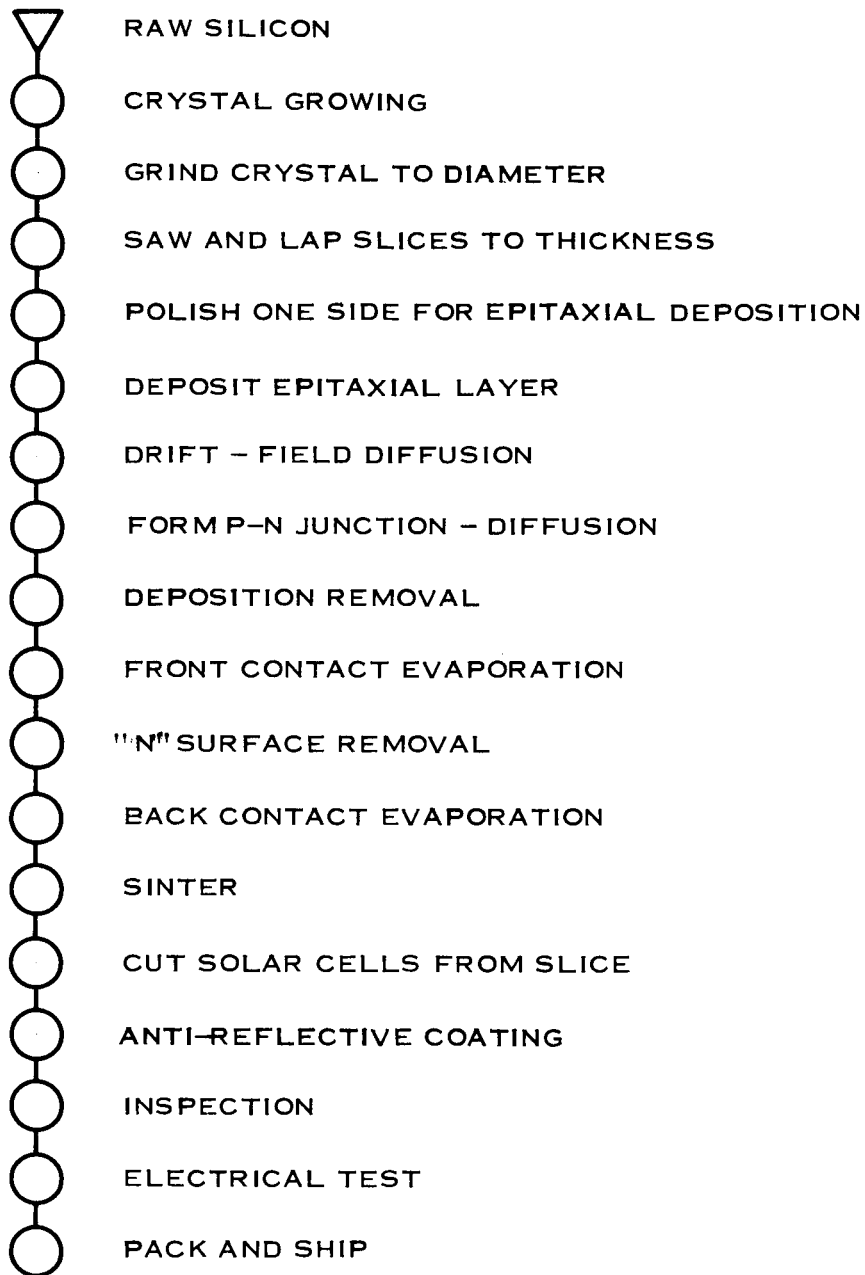
In Figure 46 is a photo of the diffused slice with an evaporated titanium silver contact on the back surface.

Figure 47 shows a photo of the diffused slice after application of the front contact.

Figure 48 shows two finished cells after the cutting operation.

A photo of the electrical test set, with the contact evaporater in the background, is shown in Figure 49.

The process fabrication techniques generally follow those used in making standard production devices. Titanium-silver sintered solderless contacts were used with a silicon monoxide antireflective coating. Phosphorus diffusant was used in all cases. Adapting the process to production should involve no large problems.

RAW SILICON

CRYSTAL GROWING

GRIND CRYSTAL TO DIAMETER

SAW AND LAP SLICES TO THICKNESS

POLISH ONE SIDE FOR EPITAXIAL DEPOSITION

DEPOSIT EPITAXIAL LAYER

DRIFT – FIELD DIFFUSION

FORM P–N JUNCTION – DIFFUSION

DEPOSITION REMOVAL

FRONT CONTACT EVAPORATION

"N" SURFACE REMOVAL

BACK CONTACT EVAPORATION

SINTER

CUT SOLAR CELLS FROM SLICE

ANTI–REFLECTIVE COATING

INSPECTION

ELECTRICAL TEST

PACK AND SHIP

SC01932

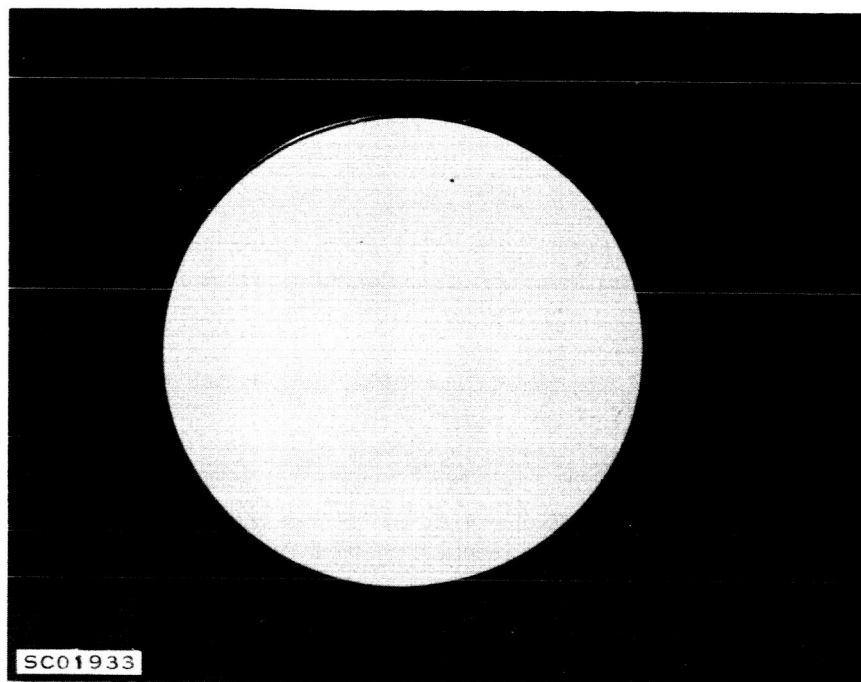Figure 44.   Fabrication Flow Diagram for Drift-field Solar Cells

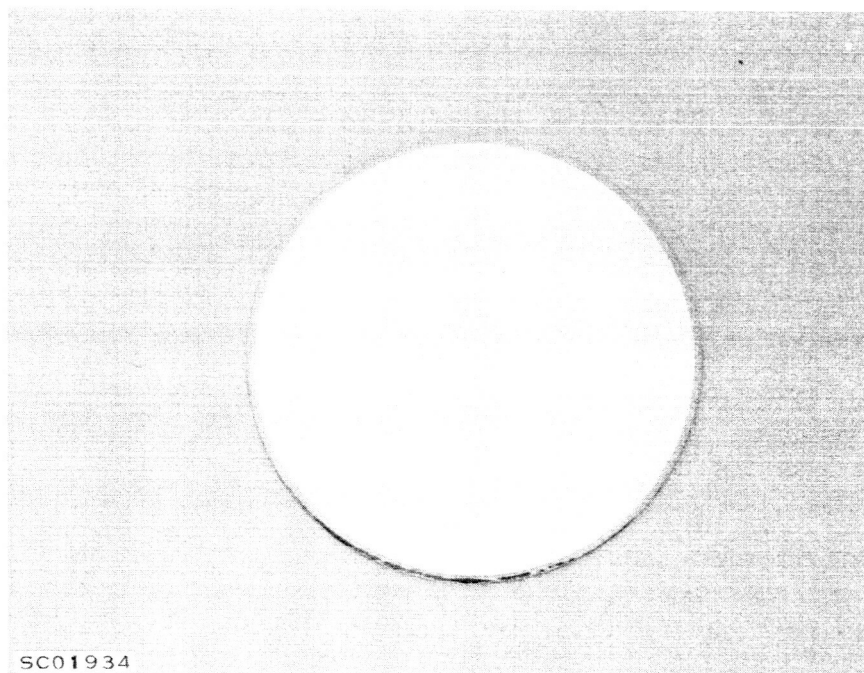Figure 45. Epitaxial Slice After Diffusion

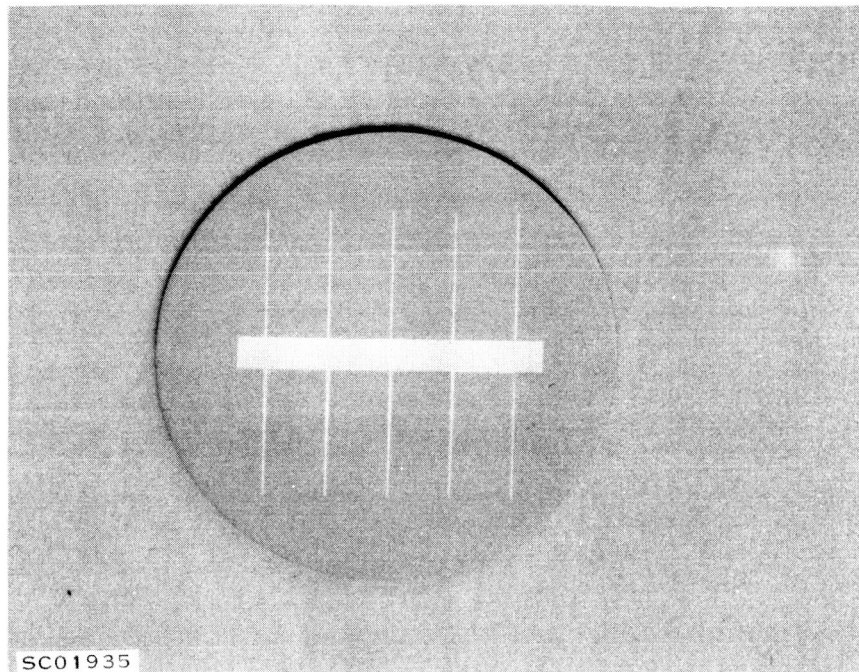Figure 46. Slice After Ti-Ag Back Contact Evaporation

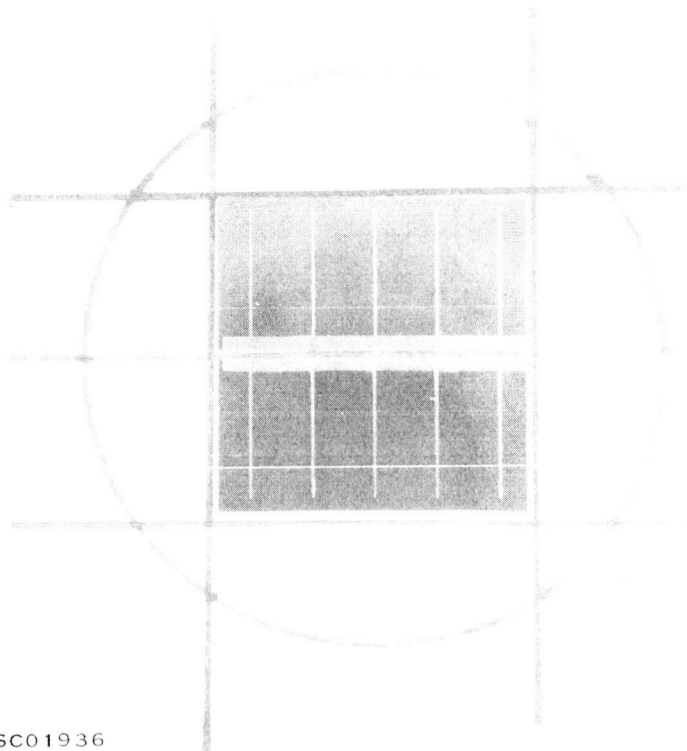Figure 47.   Slice After Ti-Ag Front Contact Evaporation

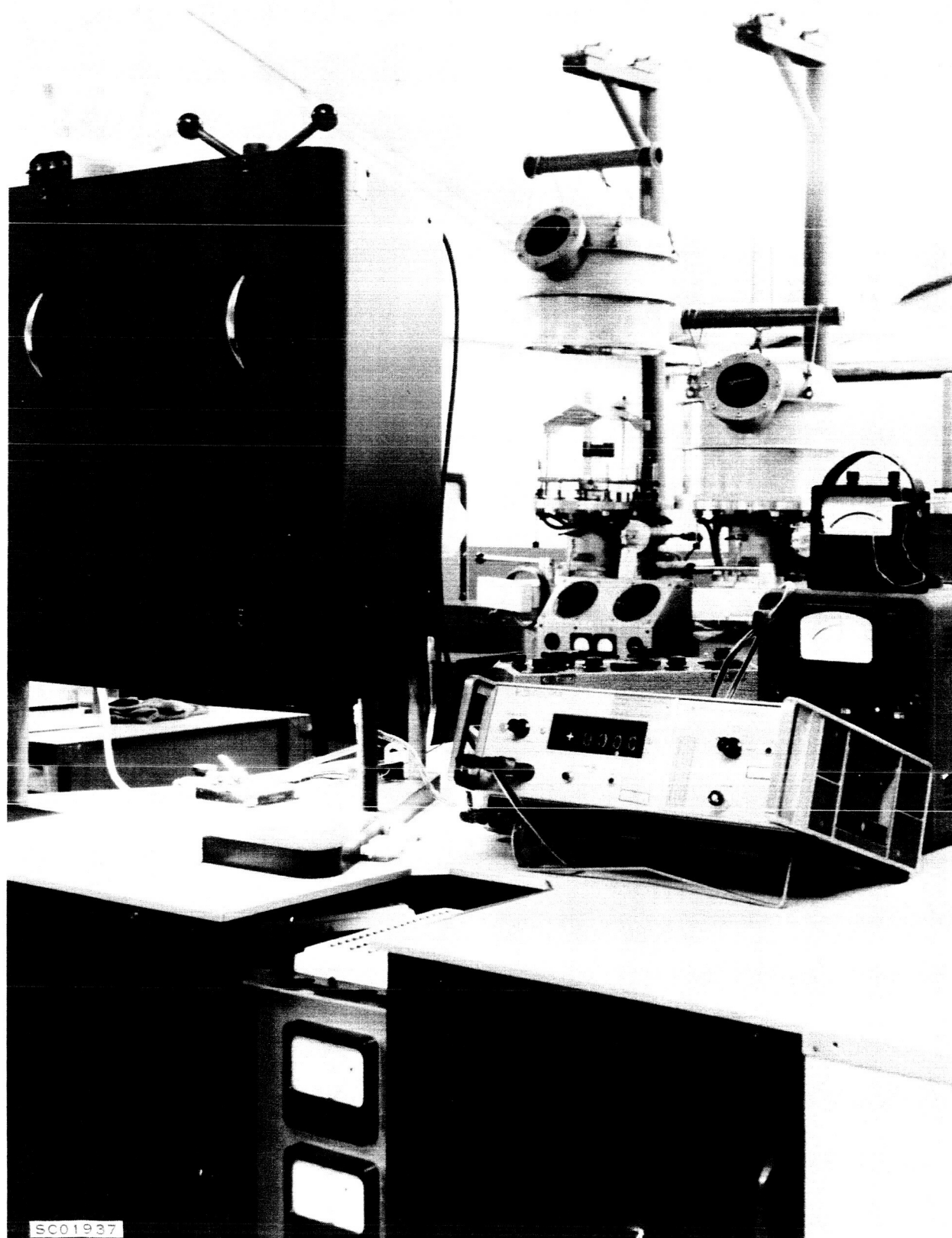Figure 48.   Finished Cells After Cutting Operation

SC01937

Figure 49.   Electrical Test Set and Contact Evaporator

SECTION VII

CONCLUDING STATEMENT

In summary, it can be said that satisfactory short-circuit current theory, field incorporation techniques, manufacturing methods and measuring methods are at hand, and that with the addition of theoretical open-circuit voltage values, a good assessment of the drift-field cell capabilities can be made. Over the range of total flux considered in this study, there appears to be little advantage in using drift-field cells.

APPENDIX I

SPECIFICATIONS FOR EPITAXIAL SOLAR CELL MATERIAL

APPENDIX I

SPECIFICATIONS FOR EPITAXIAL SOLAR CELL MATERIAL

SRDL Epitaxial Materials   Specifications for Device <u>Epi Solar Cell</u>

Date of Writing <u>10-18-65</u>   Supersedes Specification Dated _____

CRYSTAL SPECIFICATION

Pulled   <u>X</u>   Float Zoned _____

Type   <u>p</u>

Dope   <u>boron</u>

Resistivity   <u>0.055</u> to <u>0.065</u> Ω-cm, Bulk _____ Slice <u>X</u>

Xtal Orientation <u>(111)</u> Flat Orientation <u>None</u> Flat Size _____

Diameter   <u>1.187 ± 0.002"</u>   Centerless Ground   <u>Yes</u>

Lifetime   _____

Etch Pit   <u>≤ 3000/cm</u> Star Pattern <u>None</u> Slip <u>None</u>

Lineage   <u>None</u>

OTHER SPECIFICATIONS

Epitaxial Substrate   Epitaxial Layer

Slice Thickness <u>20.0 ± 0.5 mils</u> Dope   <u>Boron</u>

Sawed   <u>20.0 ± 0.5 mils</u>   Resistivity <u>8-13 ohm-cm</u>

Lapped   <u>14.5 ± 0.5 mils</u>   Thickness <u>0.94-1.02 mils</u>

Polished <u>12.5 ± 0.5 mils</u>